Bound excitons in ZnO: Structural defect complexes versus shallow impurity centers

M. R. Wagner,* G. Callsen, J. S. Reparaz, J.-H. Schulze, R. Kirste, M. Cobet, I. A. Ostapenko, S. Rodt, C. Nenstiel, M. Kaiser, and A. Hoffmann
Institute of Solid State Physics, Technische Universität Berlin, Hardenbergstrasse 36, D-10623 Berlin, Germany

A. V. Rodina
A. F. Ioffe Physico-Technical Institute, 194021 St. Petersburg, Russia

M. R. Phillips
Department of Physics and Advanced Materials, University of Technology Sydney, P.O. Box 123, Broadway, New South Wales 2007, Australia

S. Lautenschläger, S. Eisermann, and B. K. Meyer
I. Physics Institute, Justus-Liebig-University Giessen, Heinrich-Buff-Ring 16, D-35592 Giessen, Germany
(Received 24 March 2011; published 26 July 2011)

ZnO single crystals, epilayers, and nanostructures often exhibit a variety of narrow emission lines in the spectral range between 3.33 and 3.35 eV which are commonly attributed to deeply bound excitons (Y lines). In this work, we present a comprehensive study of the properties of the deeply bound excitons with particular focus on the Y_0 transition at 3.333 eV. The electronic and optical properties of these centers are compared to those of the shallow impurity related exciton binding centers (I lines). In contrast to the shallow donors in ZnO, the deeply bound exciton complexes exhibit a large discrepancy between the thermal activation energy and localization energy of the excitons and cannot be described by an effective mass approach. The different properties between the shallow and deeply bound excitons are also reflected by an exceptionally small coupling of the deep centers to the lattice phonons and a small splitting between their two electron satellite transitions. Based on a multitude of different experimental results including magnetophotoluminescence, magnetoabsorption, excitation spectroscopy (PLE), time resolved photoluminescence (TRPL), and uniaxial pressure measurements, a qualitative defect model is developed which explains all Y lines as radiative recombinations of excitons bound to extended structural defect complexes. These defect complexes introduce additional donor states in ZnO. Furthermore, the spatially localized character of the defect centers is visualized in contrast to the homogeneous distribution of shallow impurity centers by monochromatic cathodoluminescence imaging. A possible relation between the defect bound excitons and the green luminescence band in ZnO is discussed. The optical properties of the defect transitions are compared to similar luminescence lines related to defect and dislocation bound excitons in other II–VI and III–V semiconductors.

DOI: 10.1103/PhysRevB.84.035313 PACS number(s): 71.35.−y, 71.55.Gs, 78.55.Et, 78.47.jd

I. INTRODUCTION

ZnO is an actively researched semiconductor with a wide variety of potential applications in optoelectronics such as microcavity based polariton lasers[1] and adjustable UV light emitters based on ZnMgO quantum wells.[2] However, stable p doping and a rather high defect density in ZnO are the major obstacles toward the development of a large ZnO based market for light emitting devices. The main requirements for the improvement of bipolar ZnO structures are the presence of a shallow acceptor level leading to a sufficiently large hole concentration, a high hole mobility, and the reduction of shallow donor and deep defect states which promote n-type or semi-insulating materials. The latter aspect is strongly influenced by the presence of point and extended structural defects such as interstitials, vacancies, dislocations, and stacking faults that can create undesired radiative and nonradiative recombination channels and may lead to the appearance of new emission lines.

A typical candidate for such a structural defect induced optical transition is the narrow emission line at 3.3328 eV (Y_0) in photoluminescence (PL) and cathodoluminescence (CL) spectra of ZnO. This line was reported in a multitude of different ZnO samples such as substrates,[3–6] homoepitaxial[7–9] and heteroepitaxial films,[10–13] microcrystals and nanocrystals,[14–18] nanowires,[19] and quantum wells.[20] In nanomaterials the Y_0 line is only observed in structures with sufficiently large dimensions. Stichtenoth *et al.*[19] observed the Y_0 emission in ZnO nanowires with diameters greater than 100 nm, whereas it is not observed in nanowires with smaller diameters.[19,21,22] Robin *et al.*[13] detected the Y_0 transition in ZnO nanowires with diameters of about 300 nm on GaN substrates but not on sapphire substrates, where the ZnO nanowires had a diameter of about 150 nm. In ZnO nanocrystals similar observations were reported by Fallert *et al.*[15] Untreated ZnO nanocrystals with diameters between 70 and 120 nm did not exhibit the Y_0 transition. However, after annealing larger polycrystalline clusters with diameters up to 1 μm were formed and a pronounced Y_0 line could be observed.

Several controversial interpretations for the narrow emission lines around 3.333 eV are discussed in the literature including (deep) neutral donor bound excitons (D^0X) (Refs. 4,5, and 23), acceptor bound excitons (A^0X) (Ref. 10),

 ©2011 American Physical Society

nitrogen related electron-acceptor transitions (e, A_N) (Ref. 24), transitions related to intrinsic point defects such as oxygen vacancies and zinc interstitials (V_O, Zn_i) (Refs. 11 and 25), extended structural defects,[26,27] and two electron satellites (TES).[7,14,28–30] A few relevant examples of these works shall be mentioned. Schildknecht *et al.*[4] studied different ZnO substrates grown by the chemical vapor transport (CVT) method and by the hydrothermal growth technique. A strong emission line at 3.333 eV could be observed in the CVT grown samples before and after annealing, whereas it was absent in the hydrothermally grown samples. This line was attributed to an unknown deep donor bound exciton transition. Johnston *et al.*[23] observed that the same line appeared in hydrothermally grown ZnO crystals from Rubicon Technology after annealing and ion implantation with stable and radioactive Zn and Ga isotopes. Frequently, the Y_0 line is also reported in heteroepitaxial layers. Kato *et al.*[10] observed the 3.333 eV line in MBE grown ZnO on α-Al_2O_3 substrates. Based on the spectral position they ascribed the emission to the recombination of excitons bound to neutral acceptors (A^0X). Other publications attribute this emission in nominally undoped MBE grown samples to donor bound exciton transitions due to oxygen vacancies (V_O) and/or interstitial zinc (Zn_i) (Refs. 11,25 and 31). In addition, several works identify the 3.333 eV line (or peaks in close spectral proximity) as two electron satellite transitions of shallow bound excitons such as the I_4 line at 3.3628 eV. However, this identification is (in the absence of absorption measurements) ambiguous, especially if alternative candidates for the TES transitions around 3.330 eV are present[7] or a deviating temperature dependence compared to the shallow bound excitons is observed.[14] The differentiation is further complicated by energetic shifts of the emission lines due to biaxial in-plane strain as often observed in epitaxial layers.[32,33]

Despite the large quantity of PL studies showing the 3.333 eV transition, only a few publications investigate the properties of this transition in detail. So far the most extensive studies were published by Alves *et al.*[26] and Meyer *et al.*[27] In these works the 3.333 eV line was attributed to a bound exciton recombination with a thermal activation energy E_a of around 10–11 meV. This assignment was founded on the temperature dependence of the luminescence and rather fast recombination times. Based on the spot like and localized character of the luminescence band in CL images, the transition was ascribed to deeply bound excitons at structural defects. Following these reports, several authors adopted this interpretation for different ZnO samples.[15,20,34–37] However, a convergent picture concerning the defect identification and the electronic properties of the 3.333 eV line has not yet emerged as evidenced by the large variety of contradicting explanations for this emission in recent years. Even less is known about the often weaker lines between 3.33 and 3.35 eV which sporadically appear in combination with the Y_0 transition.

In this work we present a detailed analysis of deeply bound excitons and their relation to structural defects. We thereby adopt the established nomenclature for defect bound exciton lines (Y) as applied for other II–VI semiconductors. Apart from the Y_0 line at 3.3328 eV, also adjacent lines with comparable characteristics in the energy range between 3.33 and 3.35 eV are studied and identified. These are, in particular, the Y_1 line at 3.3363 eV and the Y_2/I_{12} line at 3.3465 eV. Using absorption and photoluminescence excitation measurements, we clearly distinguish between two electron satellites and bound exciton transitions. The direct comparison of the deeply bound excitons to the comparatively shallow impurity bound excitons I_0-I_{10} reveals striking differences which are discussed in detail. Based on a variety of experimental results including a study of the influence of external magnetic and stress fields, excitation spectroscopy, and monochromatic CL imaging, we develop an qualitative model of the defects and electronic states contributing to the optical transitions of defect bound excitons in ZnO. This model and its impact on the properties of deeply bound excitons are extensively discussed including a theoretical estimation of the extend of the structural defects.

II. EXPERIMENTAL SETUP

A large variety of different ZnO substrates as well as homoepitaxial and heteroepitaxial ZnO layers were investigated. Many of these samples showed pronounced luminescence features between 3.33 and 3.35 eV. For the analysis and discussion of the defect bound excitons we focus on the experimental results obtained from a commercially available ZnO sample from Cermet Inc and a nitrogen implanted ZnO single crystal from EaglePicher without limiting the general validity of the results. The Cermet sample was grown using a melt growth process whereas the EaglePicher sample was grown by the seeded chemical vapor transport method. As a reference we also discuss a hydrothermally grown ZnO substrate from Tokyo Denpa which does not exhibit any defect related luminescence lines in this energy range.

Photoluminescence measurements were performed in a liquid helium bath cryostat at 2 K. The samples were excited by the 325-nm emission line of a HeCd laser with an excitation power of 20 mW. The emitted light was dispersed by a 1-m double monochromator with a spectral resolution of 50 μeV and detected by a bialkali detector. Temperature dependent and magneto-PL measurements were conducted in a 5 T split coil magnetocryostat with variable temperature between 2 and 300 K. Uniaxial pressure measurements were performed in a self-built pressure apparatus. The uniaxial pressure load on the samples is given by the ratio of the surface area of the pressure piston to the crystal. The external pressure was fine tuned by a two stage pressure regulator with an error of 2 mbar. For the pressure dependent measurements the c axis was oriented parallel to the direction of the uniaxial pressure ($\boldsymbol{P} \| \boldsymbol{c}$). The luminescence was excited and detected from the edge of the sample in $\boldsymbol{k} \perp \boldsymbol{c}$ direction. Photoluminescence excitation spectroscopy (PLE) was performed using a dye laser containing 2-methyl-5-t-butyl-p-quaterphenyl (DMQ). The excitation wavelength for this dye was continuously tunable between 345 and 375 nm. The dye laser was pumped by the 308-nm line of a XeCl excimer laser and was operated with a pulse repetition rate of 100 Hz, a pulse duration of 20 ns, and a pulse energy of 5 μJ. For time-resolved photoluminescence (TRPL) measurements, the samples were excited using the second harmonic of a Ti:sapphire laser at 356 nm with a pulse length of 2 ps. Time-resolved data were recorded by single photon counting using a Hamamatsu R3809U-52 microchannel plate. The instrumental time resolution was

about 40 ps which allowed the determination of lifetimes down to 15 ps using deconvolution techniques. Low temperature cathodoluminescence (CL) measurements were conducted with a scanning electron microscope JEOL JSM 840 operating at 15 kV. The CL signal was dispersed by a monochromator, providing a spectral resolution of 300 μeV at 3 eV, and detected with a liquid-nitrogen cooled charge-coupled device (CCD) array. The samples were mounted in a liquid helium flow cryostat ensuring a temperature of 6 K.

III. EXPERIMENTAL RESULTS

A. Photoluminescence

The identification of different emission lines between 3.33 and 3.35 eV in the PL spectra of ZnO is not unambiguous if solely based on their spectral position since the energies of donor bound excitons (D^0X), predicted acceptor bound excitons (A^0X) (Ref. 38), and two electron satellites of the shallow donor bound excitons TES(D^0X) overlap in this energy range. The typical energy regions of the different optical transitions in the near band-edge luminescence of ZnO are displayed in a schematic drawing in Fig. 1. The vertical lines in the figure mark the energetic positions of common features in the luminescence spectra. The Y labeled area marks the range of the optical transitions which are subject of this study. It should be noted that the depicted area of the acceptor bound excitons is solely based on theoretical considerations[38] as a conclusive proof for acceptor bound exciton emissions is still missing.

Figure 2 displays the PL spectra in the range of the free and bound exciton luminescence of different ZnO samples at a temperature of 2 K. From bottom to top, we show the PL spectra of a ZnO substrate from Tokyo Denpa, a nitrogen implanted EaglePicher crystal, and a ZnO substrate from Cermet. In the energy range between 3.35 and 3.38 eV, all samples exhibit a large number of emission lines which differ in their energetic position and intensity. The luminescence lines in this range are related to the radiative recombination of the free excitons, ionized bound excitons, and neutral bound excitons and were extensively reported in the literature.[27,39] Between 3.33 and 3.35 eV several additional luminescence features are observed. In particular, these are the transition

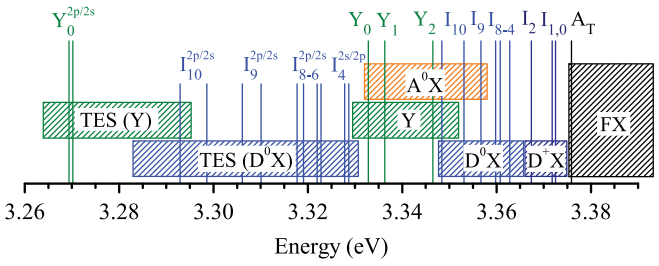

FIG. 1. (Color online) Schematic drawing of the energy ranges of various optical transitions at low temperature. Selected transitions are indicated by vertical lines. The different areas mark the energy range of free excitons (FX), ionized donor bound excitons (D^+X), neutral donor bound excitons (D^0X), acceptor bound excitons (A^0X), deeply bound excitons (Y), and two electron satellites (TES) of shallow and deeply bound excitons in their $2s$ and $2p$ states.

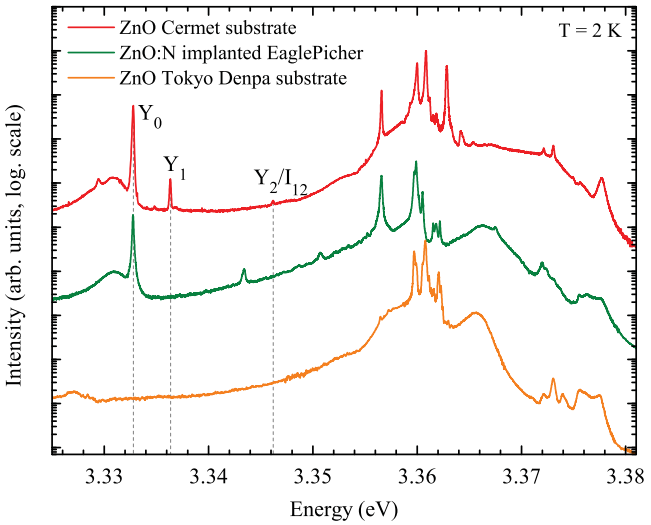

FIG. 2. (Color online) Photoluminescence spectra of different ZnO crystals at $T = 2$ K. Several narrow emission lines are visible in the spectral range between 3.33 and 3.35 eV. The strongest peaks are the Y_0 and the Y_1 lines. The spectra are vertically shifted and normalized to the dominant bound exciton line.

lines at 3.3328 eV (Y_0), 3.3363 eV (Y_1), and 3.3465 eV (Y_2/I_{12}) of which the latter emission line is only very weakly visible in the spectrum of the untreated ZnO substrate from Cermet but greatly increases in intensity after the application of uniaxial pressure (see Sec. III H). The most pronounced feature in this region is the commonly observed Y_0 line which is sometimes also labeled DBX (Ref. 27), DD (Refs. 4 and 23), or just 3.333 eV line. This line has the same energy and Gaussian line shape in different samples despite the variations in the rest of the free and bound exciton luminescence. The line width of 0.1–0.2 meV is comparable in the investigated samples although larger widths were occasionally reported in samples with broader shallow bound exciton lines. The presence of the Y_0 line in different types of samples makes its assignment to a specific dopant unlikely. This conclusion is supported by the absence of any of these lines in the Tokyo Denpa sample, even though similar luminescence features compared to the other samples are present in the free and bound exciton region. However, this fact does not exclude the possibility of structural defect bound excitons as they may appear under very different growth conditions and are independent of the bound exciton luminescence structure. In addition, defects in single crystals can be introduced by cutting, polishing or etching processes, giving rise to new localized luminescence centers which are related to structural defects close to the surface.[40] Furthermore, ion implantation often leads not only to the usually intended incorporation of dopants, but also to the creation of new structural defects which may serve as radiative recombination centers for deeply bound excitons.[23,41]

Similar considerations also apply for the Y_1 and Y_2/I_{12} transitions. In a publication of Johnston *et al.*,[23] a weak luminescence peak at an energy of 3.5 meV above the energy of the Y_0 transition was observed in ion implanted ZnO samples, but not discussed. Although, the absolute energies of the transition lines were slightly shifted, possibly due to strain,[32,33] the energy spacing between these two lines precisely matched

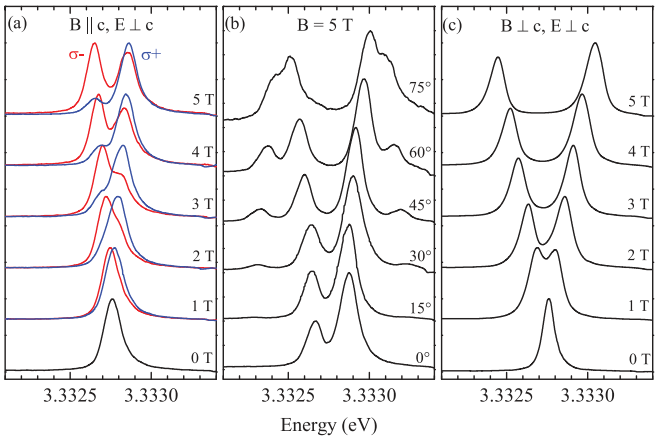

FIG. 3. (Color online) Photoluminescence spectra of the Y_0 line at 2 K for different magnetic fields, orientations and angles. (a) Faraday configuration ($\boldsymbol{B}\|\boldsymbol{c}\|\boldsymbol{k}$), (b) angles $\theta = 0°$, 15°, 30°, 45°, 60°, 75° between $\boldsymbol{B}$ and $\boldsymbol{c}$ with $B = 5$T, (c) Voigt configuration ($\boldsymbol{B}\perp\boldsymbol{c}\|\boldsymbol{k}$). Blue (dark) and red (light) lines in Faraday configuration indicate σ^+ and σ^- polarized light, respectively.

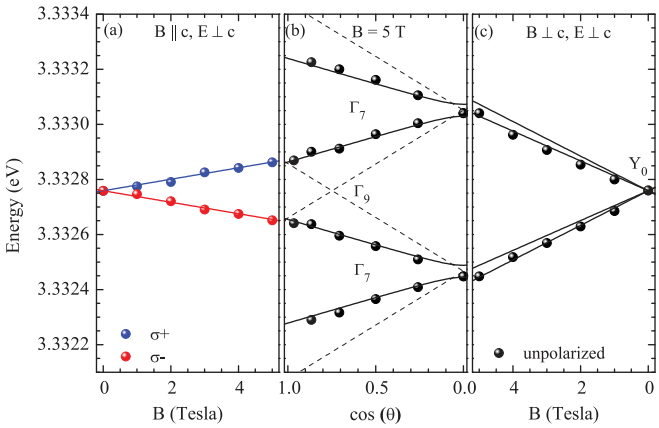

FIG. 4. (Color online) Zeeman splitting of the Y_0 line at 2 K. (a) Faraday configuration ($\boldsymbol{B}\|\boldsymbol{c}\|\boldsymbol{k}$), (b) various angles θ between $\boldsymbol{B}$ and $\boldsymbol{c}$ with $B = 5$T, (c) Voigt configuration ($\boldsymbol{B}\perp\boldsymbol{c}\|\boldsymbol{k}$). Blue and red data points indicate the peak position for σ^+ and σ^- polarized light, respectively. Black dots show the peak energies in the unpolarized measurements. Solid lines represent fits for hole states with Γ_7 symmetry, dotted lines indicate the predicted angular dependence for exciton hole states with Γ_9 symmetry. Splitting of the outer transition in (a) are not shown since they are not active for the displayed configuration but only for $\boldsymbol{E}\|\boldsymbol{c}$.

the distance between the here studied Y_0 and Y_1 features at 3.3328 and 3.3363 eV, respectively. Therefore, the small peak in this work most likely represents the Y_1 line. Only recently, the Y_2 (I_{12}) emission was studied by Brandt *et al.*[42] and Ohno *et al.*[43] and could be identified as a donor bound exciton, presumably requiring a distorted lattice structure.[42] Finally, an emission line at 3.3434 eV is observed in Fig. 2 which appeared exclusively in the nitrogen implanted ZnO sample. This line will not be further discussed in the present work, but might be related to structural defects caused by the ion implantation.

B. Defect type and charge state

To gain information about the properties of the defects involved in the Y transitions, the photoluminescence is investigated under the influence of an external magnetic field of up to 5 Tesla. Although the following discussion primarily focuses on the Y_0 line, it is equally valid for the Y_1 line. Figure 3 displays the low temperature magneto-PL spectra of the Y_0 line in the Faraday configuration $\boldsymbol{B}\|\boldsymbol{c}$ (a), for various angles θ between the directions of $\boldsymbol{B}$ and $\boldsymbol{c}$ (b), and in the Voigt configuration $\boldsymbol{B}\perp\boldsymbol{c}$ (c). The zero field spectrum shows a narrow recombination line with a full width at half maximum (FWHM) of around 120 μeV. With increasing magnetic field in the $\boldsymbol{B}\perp\boldsymbol{c}$ configuration, the Y_0 line exhibits a Zeeman splitting into two components as displayed in Fig. 3(c). The recently reported four fold splitting related to a Γ_7 hole state fine splitting in the Voigt configuration by Wagner *et al.*[44] is not resolved in these spectra. This is most likely caused by the fact that the energy splitting determined by the perpendicular hole g value $g_h^\perp$ in a magnetic field $B = 5$ T is exceeded by the spectral line width of the Y_0 transition. Consequently, it is not possible to observe the additional splitting of this line in $\boldsymbol{B}\perp\boldsymbol{c}$. In the Faraday configuration ($\boldsymbol{B}\|\boldsymbol{c}$), the emitted light possesses a pronounced circular polarization as shown in Fig. 3(a). The high energy Zeeman component has σ^+ polarization (blue lines) whereas the lower energy transition is σ^- polarized (red lines). This is consistent with previously reported magnetooptical studies of bound excitons in ZnO (Refs. 44 and 45).

The peak positions of the Zeeman components as function of the magnetic field and angle between $\boldsymbol{B}$ and $\boldsymbol{c}$ are displayed in Fig. 4. The linear splitting with increasing magnetic field in the $\boldsymbol{B}\perp\boldsymbol{c}$ orientation is characteristic of an exciton bound to a neutral defect center. In the case of an ionized complex, a nonlinear splitting due to the spin-exchange interaction would be expected.[45] This would lead to a zero field splitting as reported for dislocation bound excitons in CdS (Ref. 46) and the impurity bound exciton lines I_0, I_1, and $I_{2/3}$ in ZnO (Refs. 38,45, and 47). Evidently this is not the case for the Y_0 line [Fig. 4(c)]. From the fits of the peak positions in Fig. 4, the electron and hole g factors of the Y_0 center are derived with values of $g_e = 2.02$, $g_h^\perp = 0.15$, and $g_h^\parallel = -1.30$. These values are obtained for an isotropic electron g factor g_e and an anisotropic hole g factor g_h with

$$g_h = \sqrt{|g_h^\parallel|^2\cos^2(\theta) + |g_h^\perp|^2\sin^2(\theta)}, \quad (1)$$

where θ is the angle between the c axis and the direction of the magnetic field $\boldsymbol{B}$. The energy of the Zeeman peaks is therewith calculated to

$$E = E_0 \pm \tfrac{1}{2}\mu_B B(g_h \pm g_e), \quad (2)$$

with E_0 being the emission energy without an external magnetic field and μ_B the Bohr magneton. The electron g_e factor of 2.02 is considerable larger compared to those of shallow impurity related donor states with typical values between 1.955 and 1.958.[45,48–50] Instead, it is in excellent agreement with reported values for defects such as, for example, the Zn vacancy center, which were obtained by electron paramagnetic resonance (EPR) and optical detection magnetic resonance (ODMR).[51–54] However, the Zn vacancy

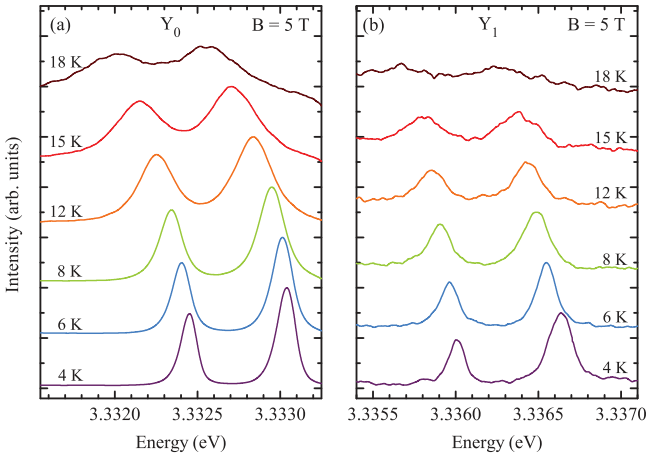

FIG. 5. (Color online) PL spectra of the (a) Y_0 and (b) Y_1 emission lines as a function of temperature between 4 and 18 K. Spectra are recorded in a magnetic field of $B = 5$ T with $\boldsymbol{B}\perp\boldsymbol{c}$.

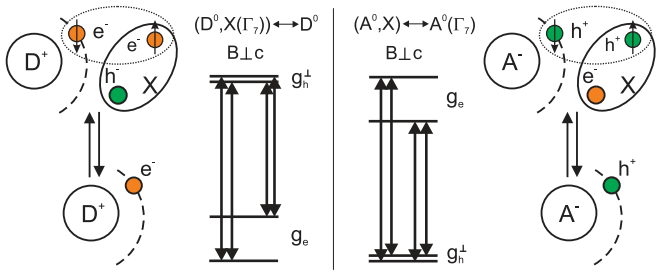

FIG. 6. (Color online) Zeeman splitting of neutral donor and acceptor bound exciton complexes involving Γ_7 electron and hole states in a constant external magnetic field with $\boldsymbol{B}\perp\boldsymbol{c}$. The g values in the ground and excited states depend on the spin of the unpaired particles. The depicted models also apply for any complex involving two electrons and one hole (donor complex) or one electron and two holes (acceptor complex), even if the core centers are different from D^+ or A^-, respectively.

itself cannot be responsible for the Y_0 emission line as it forms a deep acceptor state in ZnO.[55–57]

Following the determination of the charge state and g values, we will now address the question if the Y_0 and Y_1 transitions involve hole states from the A or B valence band. Thereto, the angular dependent energy shift of the Y lines in a magnetic field is analyzed in Fig. 4(b) (not shown for the Y_1 line). In agreement with previous angular resolved magnetooptical studies of neutral bound excitons in ZnO (Refs. 44 and 45), the energetic shift of the Y lines show no crossing of the inner two Zeeman components. Consequently, the bound excitons Y_0 and Y_1 involve holes from a valence band with Γ_7 symmetry, since Γ_9 hole states would lead to an angular crossing at around 40° in Fig. 4(b). In light of a recent study of the valence band ordering in ZnO by Wagner *et al.*[44] which proved the originally proposed Γ_7, Γ_9, Γ_7 symmetry ordering by Thomas and Hopfield,[58] it is evident that both Y recombinations involve hole states from the topmost (A) valence band with Γ_7 symmetry.

Figure 5 displays the temperature dependent PL spectra of the Y_0 and Y_1 lines under the influence of a magnetic field of 5 T in the $\boldsymbol{B}\perp\boldsymbol{c}$ configuration. Both lines show a rapid intensity decrease with increasing temperature between 4 and 18 K. Based on the analysis of their thermalization behavior in an external magnetic field, the emission lines can be attributed to donor or acceptor bound excitons. Thereto, the different splittings for neutral donor and acceptor bound excitons with Γ_7 hole state symmetry have to be analyzed. The corresponding energy level schemes in the Voigt configuration with $\boldsymbol{B}\perp\boldsymbol{c}$ are displayed in Fig. 6. In the case of a donor bound exciton, the splitting of the ground state is determined by the electron g value g_e, whereas the splitting of the excited state is given by the much smaller hole g value $g_h^{\perp}$. For an acceptor bound exciton this order is reversed [Fig. 6(b)]. Apparently, the intensity ratio of the two Zeeman components shows no significant changes with rising temperature for both lines. Since the thermalization in luminescence depends exclusively on the splitting of the excited state, the constant PL intensity ratios indicate that no sufficient splitting of the excited state is present to cause a pronounced thermalization (increasing intensity of the high energy component). Such a behavior is expected for a donor and confirms the attribution of the Y lines to donor bound exciton recombinations.

It is important to note that the observed linear splitting in the Voigt configuration will occur not only for excitons bound to isolated neutral impurities, but for any complex involving two paired and one single charge carrier. Thus, the magneto-PL and temperature dependent data for the Y_0 and Y_1 lines only proof that these transitions originate from complexes involving two electrons and one hole of Γ_7 symmetry, but do not provide additional information about the origin of the complex center. However, if these complexes would possess singly charged D^+ cores like shallow impurity bound excitons, one would expect much larger donor binding energies for these centers compared to previously studied shallow donor bound exciton lines.[27,38] Alternative models based on the experimental data are discussed in Sec. IV.

C. Activation and localization energies

Aside from the identification of excitons bound to donors or acceptors based on temperature dependent PL in magnetic fields, the study of the energetic shift as function of temperature in zero field provides additional information which reveal fundamental difference between the shallow and deep exciton binding centers. The most significant contribution to the energy shift of excitons bound to shallow impurity states is usually given by the temperature dependence of the band edge. Several models which describe this energy shift are found in the literature.[59–62] Although the empirical Varshni equation[59] is often applied, it should be considered that the Varshni model involves certain deficiencies such as a systematic deviation in the cryogenic temperature region and a high instability of the Varshni parameter set.[62] In particular, the Varshni model is inadequate if the investigated temperature range is much lower than the Debye temperature of 920 K in ZnO (Ref. 63). Since the deeply bound exciton lines already disappear at temperatures above 25 K (Fig. 5), the Varshni model is not applicable in this case. Therefore, the temperature dependence is computed by a model suggested by Viña *et al.*,[61,64] which is based on a Bose-Einstein model and delivers a more reliable description in the low temperature range.

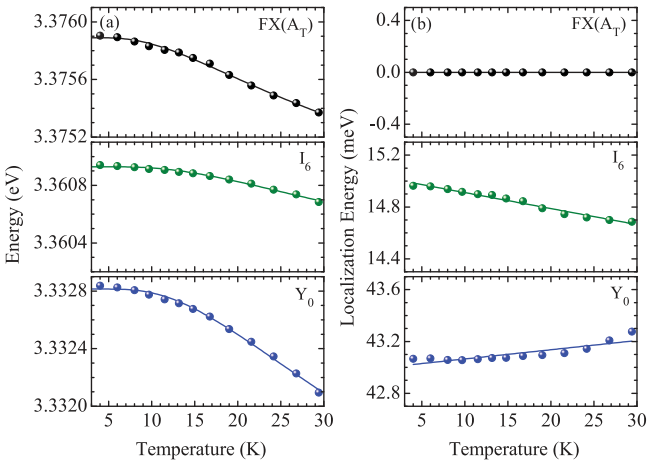

FIG. 7. (Color online) Energy shift of the FX(A_T), I_6, and Y_0 lines as function of temperature between 4 and 30 K. The shift is displayed for (a) absolute energies and (b) localization energies. Solid lines represent fits based on (a) a Bose-Einstein model (Refs. 61 and 64) and (b) linear fits.

Figure 7(a) displays the experimentally determined spectral position of the FX(A_T), I_6, and Y_0 lines as function of temperature. The solid lines indicate least-squares fits to the experimental data. Although the calculated parameters have large uncertainties due to the limited temperature range, it is evident that the free excitons, shallow bound excitons, and deeply bound excitons exhibit different energy shifts as function of temperature. Nevertheless, the temperature dependence of the longitudinal and transversal free excitons [FX(A_L), FX(A_T)], the shallow bound excitons (I_i), and the deeply bound excitons (Y_i) is found to be equal within each group.

The distinction between the temperature dependence of different free and bound exciton transitions is usually not reported and analyzed in other temperature dependent studies of the near band edge luminescence in ZnO. Typically, temperature dependent measurements cover the full range from liquid helium temperature up to room temperature and above.[65–67] In view of the large temperature region, most works show only very few temperature steps between 2 and 30 K. In addition, a high spectral resolution at low temperatures might be considered circumstantial for a temperature series due to the increased line width at elevated temperatures which is caused by the dissociation of bound excitons and broadening of free excitons. Consequently, a precise analysis of the temperature dependence of the different exciton transitions in the low temperature range would not be possible. All these problems were avoided in this work by recording PL spectra of the free and bound excitons with temperature steps of 2 K and a spectral resolution better than 50 μeV, thus enabling the distinction between all observed exciton lines.

The large discrepancy in the temperature shift between the Y_0 and I_6 contradicts the assignment of the Y lines to shallow bound excitons. This becomes even more evident if the temperature dependence of the localization energy is analyzed as plotted in Fig. 7(b). The localization energy E_{loc} is defined as the energy spacing between the bound excitons and the free transversal A exciton FX(A_T). Thus, the localization energy of FX(A_T) is constant by definition with $E_{\mathrm{loc}} = 0$. For the shallow bound excitons (e.g., I_6), a pronounced decrease of the localization energy is observed with increasing temperature. Such a temperature dependence is typical for the shallow bound excitons and can be explained by the screening of the impurity potential caused by the increasing free carrier concentration with rising temperature. In contrast, the Y lines exhibit a stronger red shift compared to the other exciton lines resulting in an increase of the localization energy with increasing temperature. The observed temperature dependence of the Y lines also indicates that the description of these centers requires a different model than for shallow impurity bound excitons. This necessity is further emphasized by a study of the binding energies of these excitons which are determined by fitting the peak intensities as a function of the reciprocal temperature in an Arrhenius plot. Despite the large localization energies of $E_{\mathrm{loc}} = 43.1$ and 39.6 meV for the Y_0 and Y_1 exciton lines, respectively, a thermal activation energy $E_a \approx 12 \pm 2$ meV is derived for both centers. This energy is in agreement with reported values of 10–11 meV for the Y_0 line.[11,26,27] By contrast, the thermal activation energies of the shallow bound excitons approximately coincide with the localization energies. The small thermal activation energies $E_a < E_{\mathrm{loc}}$ observed for the Y lines suggest that the respective defect centers, in contrast to the shallow donors, do not bind the exciton as a whole quasiparticle, but rather as separate electron and hole connected by the Coulomb interaction. As result, the lowest ionization potential of such a complex—the thermal activation energy—does not correspond to the detachment of an exciton but to the detachment of only one of the particles of the complex (electron or hole). Possible models of the binding centers for these three-particle complexes (two electrons and one hole) are discussed in Sec. IV.

D. Phonon replica and two electron satellites

Figure 8 displays the low temperature PL spectra of the Cermet and EaglePicher samples in comparison to the

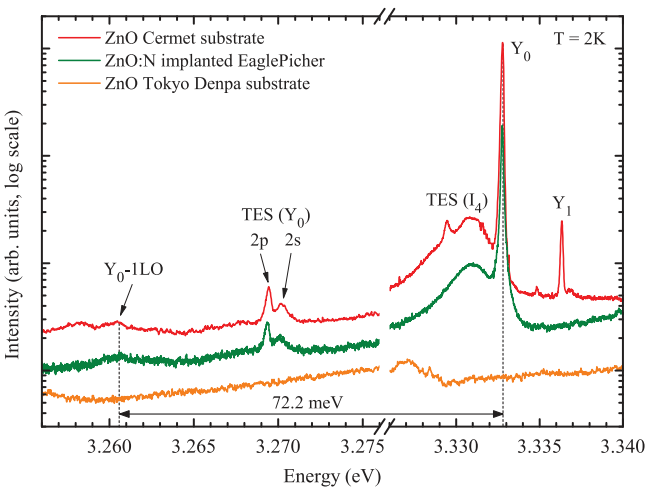

FIG. 8. (Color online) PL spectra of Y lines with the 1LO phonon replica and two electron satellites of the Y_0 line. The LO and TES features are not observed in samples without pronounced Y_0 line (Tokyo Denpa substrate).

substrate from Tokyo Denpa which does not exhibit any Y lines. At the low energy side of the Y_0 line, a weak luminescence sideband with a maximum at 3.2606 eV is observed for the two samples with pronounced Y_0 emission. The energy spacing to the Y_0 line at 3.3328 is 72.2 meV, precisely matching the energy of the longitudinal-optical (LO) phonons in ZnO (Ref. 68). The fact that this luminescence band is only present in samples with a strong Y_0 line supports its assignment to a phonon replica. From the intensity ratio of the different LO-phonon replicas, the Huang-Rhys factor S[69] can be determined by the Poisson distribution[70,71]

$$I_n = \exp(-S)\frac{S^n}{n!}, \tag{3}$$

where $n = 0$ corresponds to the zero-phonon line (ZPL) and n is the number of the phonon replica. The parameter S determines the mean number of created phonons and therefore describes the coupling strength of an electronic transition to the longitudinal optical polarization field. For the Y_0 transition, we derive a Huang-Rhys factor of $S = 0.004 \pm 0.002$ (Table I). This value is exceptionally small in relation to the spectral position of the Y_0 line below the band gap.

For free excitons, the value of the Huang-Rhys parameter is usually overestimated if based on the intensity of the zero-phonon line I_0 (not to be confused with the bound exciton line I_0 which is related to an ionized Al impurity[38]). The reason for this overestimation is the large absorption in the range of the free excitons which results in an increased I_n/I_0 ratio. In the case of strongly localized excitons, the opposite effect may occur as not all excitons contribute to phonon replicas.[20,72] This effect can result in the determination of too small values of S, particularly in confined structures such as quantum dots and quantum wells. Consequently, only the intensities of the phonon replicas without the ZPL should be analyzed. Unfortunately, this is not possible for the Y_0 line as no 2 LO phonon band is observed due to the extraordinary weak coupling. Since the energetic positions of the Y lines are far off the absorption edge of ZnO, we can exclude an overestimation of the Huang-Rhys parameter due to absorption. Concerning the latter effect, an influence of confinement cannot be completely ruled out due to the localization of the bound excitons. Consequently, the real Huang-Rhys parameter might be larger than the determined value, however, certainly not more than one order of magnitude[72] which would still represent a very weak coupling.

The small Huang-Rhys parameter for the Y_0 transition seems to be related to the small thermal activation energy discussed in the previous section. Usually, the value of S is expected to increase as function of the localization energy.[70,73,74] To verify the validity of this relation for the Y_0 line, we compare the Huang-Rhys factor of the Y_0 line with those of the three dominant bound excitons I_4, I_6, and I_9 in the Cermet sample. The presence of up to four phonon replicas for these lines enables a reliable determination of their Huang-Rhys parameters. Using Eq. (3), we derive S values of 0.052 (I_4), 0.058 (I_6), and 0.067 (I_9) by least-squares fits which demonstrate the increasing phonon coupling with increasing localization energy (Table I). Apparently, the exceptionally small Huang-Rhys factor of the Y_0 center violates the discussed relation with respect to its large localization energy. The weak coupling of the Y lines can be explained if they involve excitonic recombinations at extended defects, within which strong delocalization of the binding potential occurs as suggested by Dean for the Y and Z lines in ZnSe (Ref. 75). This property of the extended defect is discussed in Sec. IV where different models for the binding centers of the Y lines are considered.

Apart from the weak 1 LO sideband another luminescence structure on the low energy side of the Y_0 line is apparent in Fig. 8. At 3.2702 and 3.2694 eV, two peaks are observed which are not present in samples without the Y_0 line. Based on this exclusive appearance in combination with the Y_0 line, a correlation between these peaks is evident. We identify these lines as the $2s$ and $2p$ TES transitions of the Y_0 complex. The energy spacing of the bound exciton lines to the TES $2p$ states as well as the size of the $2s$-$2p$ splitting are listed and visualized for the excitons I_4 to I_{10} and the Y_0 in Table I and Fig. 9. The $1s$-$2p$ and $2s$-$2p$ splitting increase linearly as function of the localization energy E_{loc} for the shallow bound excitons I_4 to I_{10} (Ref. 27). Note, that the localization

TABLE I. Energy of shallow and deeply bound excitons and their two electron satellite transitions. E_{loc} denotes the localization energy of the bound excitons according to Ref. 27, E_a their thermal activation energy, E_D the donor binding energy, TES($2s$) and TES($2p$) the energies of the two electron satellites in the $2s$ and $2p_{x,y}$ states, $E(1s\text{-}2p)$ and $E(2s\text{-}2p)$ the energy spacing between the exciton line and the specified TES transition and S the Huang-Rhys parameter.

Exciton	Energy E (eV)	E_{loc} (meV)	E_a (meV)	E_D (meV)	TES($2s$) (eV)	TES($2p$) (eV)	$E(1s\text{-}2p)$ (meV)	$E(2s\text{-}2p)$ (meV)	S
I_4	3.3628	13.1	13	46.1	3.3278	3.3287	34.1	−0.9	0.052
I_6	3.3608	15.1	15	51.5	3.3228	3.3220	38.8	0.8	0.058
I_8	3.3598	16.1	16	54.6	3.3191	3.3177	42.1	1.4	–[d]
I_9	3.3567	19.2	19	63.2	3.3101	3.3061	50.6	4.0	0.067
I_{10}	3.3531	22.8	23	72.6	3.2986	3.2929	60.2	5.7	–[d]
Y_1	3.3363	39.6	12	–[a]	–[b]	–[b]	–[b]	–[b]	–[d]
Y_0	3.3328	43.1	12	-[a]	3.2702[c]	3.2694[c]	63.4[c]	0.8[c]	0.004

[a]These centers cannot be described by an effective mass approach. Models and values are discussed in Sec. IV.
[b]No TES states are observed due to the small intensity of the Y_1 line.
[c]Electronic configuration of the excited states might be different for Y centers (defect complexes).
[d]No matching phonon replica are observed.

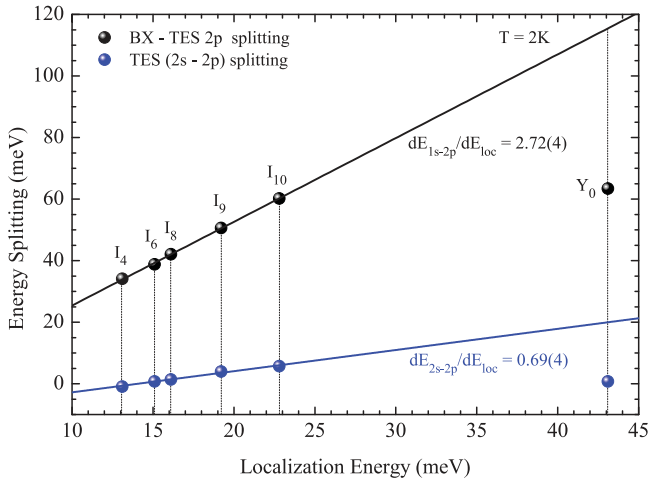

FIG. 9. (Color online) Energy splittings of bound excitons and TES states for shallow bound excitons (Ref. 27) and the Y_0 exciton line.

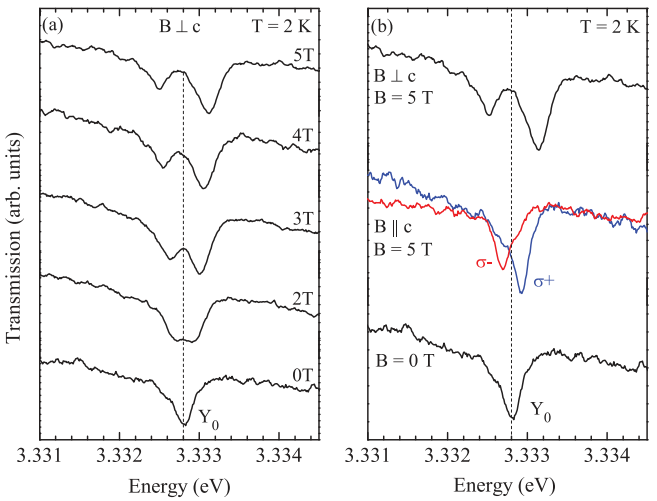

FIG. 10. (Color online) Magnetooptical transmission spectroscopy of deeply bound excitons in N implanted ZnO single crystals. (a) Voigt configuration ($\boldsymbol{B}\perp\boldsymbol{c}\|\boldsymbol{k}$) with magnetic field strengths between 0 T and 5 T. (b) Top: $\mathbf{B}\perp c$ at 5 T, center: $\mathbf{B}\|c$ at 5 T with polarization directions σ^+ and σ^-, bottom: zero-field transmission. All spectra are recorded at 2 K.

energies listed in Table I are determined from the transversal free exciton energy FX(A_T) at 3.3759 eV according to Meyer *et al.*[27] However, in the samples under investigation, the position of the FX(A_T) are slightly shifted by not more than 500 μeV resulting in small variations of the localization energies and TES positions. In contrast to the I lines, the TES spacing of the Y_0 does not follow the discussed relation in Fig. 9. Instead, significantly smaller values for the $1s$-$2p$ and $2s$-$2p$ splitting are obtained. The size of the $1s$-$2p$ splitting of the Y_0 complex indicates the small binding energy of the electron in the complex ground state which seems to be similar to those of the shallow donor I_{10} (Table I). At the same time, the $2s$-$2p$ splitting for the Y_0 line is smaller than those for the I_{10}. The fact that the TES splitting of the Y_0 complex does not follow the relation for the I centers provides important information concerning the possible defect complexes as discussed in detail in Sec. IV.

Similar luminescence features to the LO and TES lines of the Y_0 were also reported by Wang *et al.*[34] in ZnO crystals grown by EaglePicher using the seeded chemical vapor transport method. These samples showed, apart from the Y_0 emission, weak emission lines at 3.26 and 3.27 eV. Both lines disappeared at a temperature above 15 K in agreement with our study of the temperature dependence of the Y_0 line. Despite the mismatching LO phonon energy, the 3.27 eV emission was attributed to a phonon sideband of the Y_0 transition.[34] Instead we suggest that in agreement with our study, the 3.26 eV line originates from the first LO phonon replica with an energy spacing of about 73 meV and that the 3.27 eV emission in the work of Wang *et al.* may originate from the not resolved $2s/2p$ two electron satellite transitions of the Y_0 line.

E. Magnetoabsorption

The attribution of the Y_0 emission line to a deeply bound exciton is inconclusive if solely based on luminescence studies. The difficulties in an unequivocal identification arise mainly from the energetic proximity to the two electron satellites of the dominant shallow bound excitons. These features may also possess narrow transition lines in the same spectral range and exhibit a similar thermal dependency. Several authors reported a TES emission line of the hydrogen donor bound exciton I_4 in close energetic proximity to the Y_0 transition.[28,29] In fact, we also observe pronounced TES lines around 3.330 eV in Fig. 2. To distinguish these transitions from the deeply bound exciton lines, absorption measurements are of great use. Due to the nature of the TES lines which occur if a donor is left in an excited state after the recombination of a bound exciton, these lines will not appear as absorption lines in transmission spectroscopy.

Figure 10 shows the transmission spectrum of the nitrogen implanted ZnO single crystal from EaglePicher in the energetic range of the Y_0 transition. In addition to the zero field spectrum, absorption spectra are displayed for variable external magnetic field strengths up to 5 T. In the zero-field spectrum a strong absorption line appears at 3.3328 eV which precisely matches the transition energy of the in the Y_0 in the PL spectra (Fig. 2). The presence of this line in the absorption and emission spectra excludes the possibility of a two electron satellite transition as its origin. In an external magnetic field $\boldsymbol{B}\perp\boldsymbol{c}$, the splitting of the Y_0 line into two Zeeman components is clearly visible. The size of the splitting for a given magnetic field strength is in excellent agreement with the observed splitting in the magneto-PL spectra in Fig. 3(c). From the intensity ratio of the two Zeeman components in Fig. 10(a), it is obvious that the lower energy peak decreases in intensity with increasing magnetic field compared to the higher energy absorption line. The observed magnetic thermalization can only be explained if the dominant splitting in Fig. 6 exists in the ground state and not in the excited state of the bound exciton complex. With increasing magnetic field the ground state splitting increases leading to a lower occupation of the higher energy ground state level at low temperatures. This leads to the observed decrease in the intensity of the low energy absorption line. Consequently, the magnetic thermalization in absorption provides additional evidence that the Y_0 exciton is

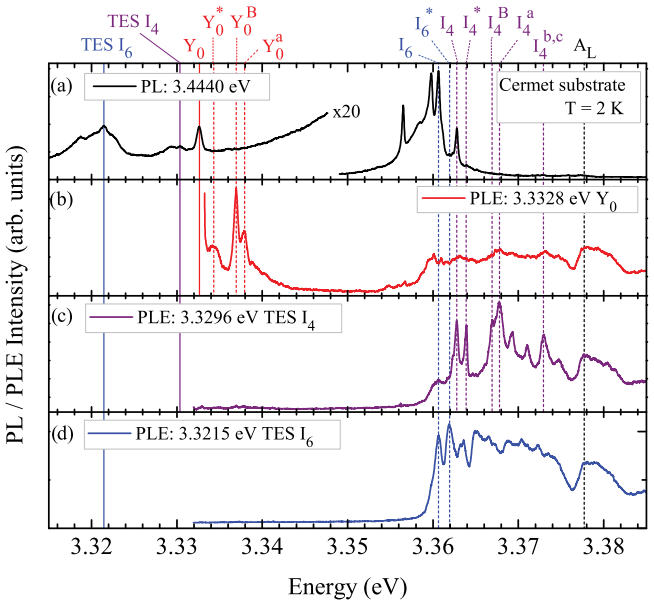

FIG. 11. (Color online) PL and PLE spectra of the ZnO Cermet substrate at $T = 2$ K. (a) PL spectrum excited by a pulsed tunable dye laser at an energy of 3.4440 eV, (b)–(d) Excitation spectra of Y_0, I_4 TES, and I_6 TES.

bound to a donor complex (Fig. 6). The same argumentation also applies for the Y_1 transition.

F. Excited states

For a detailed analysis of the bound exciton excited states and energy transfer processes, the excitation channels of the different emission lines are studied by photoluminescence excitation (PLE) spectroscopy. Figure 11(a) shows the PL spectrum of the ZnO Cermet substrate, excited by a pulsed tunable dye laser at an energy of 3.4440 eV. Solid vertical lines mark the PL peaks for which the PLE spectra are shown. The excitation channels of the Y_0 line [Fig. 11(b)] are compared with those of the two electron satellite transitions of the I_4 [Fig. 11(c)] and I_6 (Fig. 11(d)). The TES transitions exhibit a large quantity of narrow excitation channels in the range of the shallow donor bound excitons. The strong excitation peak with the lowest energy in each of the TES spectra represents the ground state of the related exciton transition. These excitation channels are observed at 3.3628 (I_4) and 3.3608 eV (I_6) in agreement with the energy of these excitons in the PL spectrum as indicated by the dashed lines. The excitation channels at the high energy side of these lines are equal to the excited states of the related bound excitons I_4 and I_6 as shown by the values in Table II. The observed excitation resonances can be divided into groups according to the different excitation mechanisms involved.[76,77] With the lowest energy spacing, the vibrational and rotational states of the excitons (D^0,X_A) are observed (1–2 meV). Since the difference between these energy levels are not resolved, the vibrational-rotational states are summarized to one energy level which is labeled Y_i^* or I_i^* in Fig. 11 and Table II. The next group of excitation channels is observed at an energy spacing between 4.1 and 4.5 meV. This distance is close to the reported energy distance of the A and B valence bands of 4.7 meV at the Γ point.[38,78] In fact, a recent study of excited state properties of donor bound excitons by Meyer *et al.*[77] revealed a spacing between the recombination lines of bound excitons involving A and B valence band holes of 4.5 meV for the I_6 to I_9 and about 4.1 meV for the I_4. Evidently, the same excitation channels are observed for the corresponding TES transitions. Thus, these excitation resonances originate from the formation of an exciton with a hole from the B valence band (D^0,X_B). The third group of excitation channels consists of electronic excited states of the exciton with energy spacings greater than 5 meV[77] which can be theoretically modeled following a formalism presented by Puls *et al.*[79] for donor-exciton complexes in CdS. Finally, energy transfer also occurs via the free excitons above 3.375 eV.

Similar to the shallow bound excitons and their two electron satellites, the excitation band in the range of the free A and B excitons demonstrates the efficient excitation of the Y_0 line by the capture of free excitons. However, in the range of the shallow bound excitons, only a weak and broadly distributed excitation band is observed. In particular, no sharp excitation channel at the energy of a specific bound exciton in this region is observed. This demonstrates that the Y lines are not related to any other impurity bound excitons and clearly differentiates these transitions from the adjacent two electron satellites. The most striking features in the excitation spectrum of the Y_0 line are the strong excitation resonances at energy spacings of 1.2, 4.1, and 5.1 meV. These lines are comparable to the excitation channels of shallow bound excitons and are attributed to

TABLE II. Excited states of the defect bound exciton Y_0, the impurity bound excitons I_4 and I_6 and their two electron satellite transitions I_4 TES and I_6 TES. (D^0,X) labels the donor bound exciton in the $1s$ ground state and TES($2p$) denotes the $2p_{x,y}$ donor excited state (Ref. 27). The excited state energies are given in relation to the (D^0,X) ground state energy. Experimental values are determined by the PLE spectra shown in Fig. 11. Theoretical values are provided as calculated in Ref. 77 All values are given in meV.

			I_4 (D^0,X)			I_6 (D^0,X)	
	Y_0 (D^0,X) (exp.)	I_4 TES($2p$) (exp.)	(exp.)	(calc.) (Ref. 77)	I_6 TES($2p$) (exp.)	(exp.)	(calc.) (Ref. 77)
I_i^*	1.2	1.1	1.1	1.06	1.3	1.4	1.32
I_i^B	4.1	4.1	4.1		4.5	4.5	
$I_i^a(0,1)$	5.1	5.1	5.2	5.8	5.9	5.9	5.9
$I_i^b(1,1)$		10.2	10.3	11.9	11.6	11.5	12.1
$I_i^c(0,2)$		10.2	10.3	12.0	11.6	11.7	12.4

vibrational-rotational excited states (Y_0^*), an exciton involving a hole from the B valence band (Y_0^B), and the first electronic excited state $Y_0^a(0,1)$. The values in brackets (see also Table II) denote the orbital and angular momentum quantum numbers of the exciton. Apparently, the (0,1) excited state of the Y_0 line has the same energy spacing (5.1 meV) as the (0,1) excited state of the I_4, whereas larger values of the excited states are found for stronger localized excitons such as the I_6. Based on the energy of the (0,1) excited state, higher electronic excited states of the Y_0 line should be expected with a splitting larger than 10 meV. However, no excitation channels are observed in this range. The absence of higher excited states correlates with the small thermal activation energy of about 12 meV since higher energies result in the detachment of a weakly bound hole as discussed in Sec. IV. Furthermore, the large intensity of the Y_0^B excitation line indicates that the capture of a free hole at the defect complex constitutes an efficient alternative excitation channel apart from the energy transfer from free excitons.

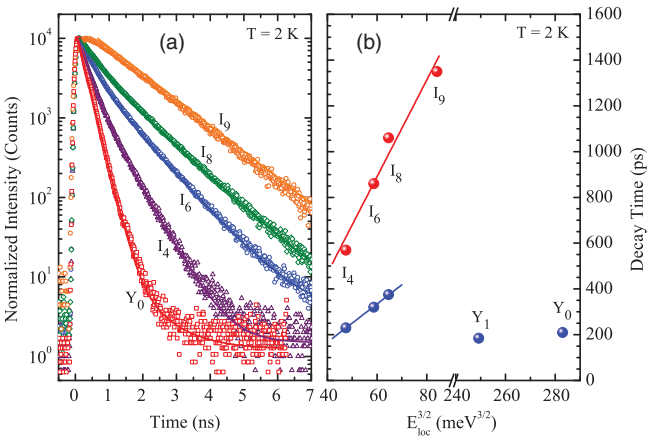

FIG. 12. (Color online) (a) Transients of the bound excitons I_4, I_6, I_8, I_9, and Y_0 at 2 K. (b) Lifetimes as function of the localization energy: dots indicate measured values, solid lines represent fits based on the model by Rashba *et al.*[82]

G. Recombination dynamics

The question arises if the different excitation mechanisms also affect the excitation and recombination dynamics of the shallow and deeply bound excitons. To address this issue, time-resolved photoluminescence spectroscopy is performed. In general, time-resolved spectroscopy can provide information about the dynamical processes including the excitation, recombination, relaxation, and dephasing processes. The lifetimes of the excitonic transitions are commonly used as indicator for the defect density of the samples.[80] Therefore, many works investigate the decay dynamics of the free exciton luminescence at room temperature. These lifetimes differ significantly in bulk samples, epilayers and nanostructures. The longest reported lifetimes of the free exciton emission in ZnO are 3.8 ns for the nonradiative process in ZnO epilayers,[30] a biexponential decay with lifetimes of $\tau_1 = 1$ ns and $\tau_2 = 14$ ns in single crystals,[80] and a lifetime of up to 27.7 ns in ZnO tetrapods.[81] To compare the dynamics of the different bound exciton transitions, room temperature measurements are not applicable as the bound excitons in ZnO typically dissociate at temperatures above 60 K. Consequently, we study the recombination dynamics of the various bound exciton transitions by time-resolved photoluminescence (TRPL) at a temperature of $T = 2$ K.

Figure 12(a) displays the transients of the impurity bound exciton lines I_4 to I_9 as well as the deeply bound exciton Y_0 together with the corresponding least-squares fits. The bound exciton lines I_4, I_6, and I_8 are well described by a biexponential decay function $A_1\exp(-t/\tau_1) + A_2\exp(-t/\tau_2)$ with a fast decay constant τ_1 between 230 and 375 ps and a slow decay constant τ_2 of 570 to 1060 ps. The lifetimes and their amplitude ratio A_2/A_1 are listed in Table III. This ratio increases toward longer lifetimes which expresses the increasing impact of the long time constant for excitons with larger localization energy. The biexponential decay indicates that a second decay channel is present at the initial stage in addition to the exciton recombination and that this channel saturates after a certain time period.[83,84] In the case of the shallow bound excitons, the initial channel might be the (nonradiative) capture process of the excitons to deeper centers (traps).[84] This process is characterized by the time constant τ_{cap} and saturates when all traps are occupied. This suggests that τ_{cap} is much smaller then the lifetime of the excitons at these traps. Therewith, the observed decay time τ_1 at the initial stage corresponds to the combined effects of recombination and capture processes $1/\tau_1 = 1/\tau_{rec} + 1/\tau_{cap}$, whereas the second time constant τ_2 corresponds to the recombination time τ_{rec}.

For the I_9 bound exciton, only the long time constant τ_2 is observed with a monoexponential decay time of 1.35 ns. In addition, a rise time τ_{rise} of 200 ps occurs for the I_9 bound exciton which corresponds to the nonradiative relaxation time of free excitons determined by capture and trapping processes at the impurities.[83,85] The fact that no rise time for other shallow bound exciton centers is observed indicates that the capture process of the free excitons to these centers is rapidly saturated and replaced by the recapture process of the excitons to deeper traps as described above. In the case of the I_9 bound exciton, two reasons might enable the observation of the rising time. First, the initial capture of the free excitons might be slower for the deeper D^0 donor (I_9) compared to the shallower ones (I_4 to I_8). Second, an additional excitation channel exists for the creation of neutral donors D^0 and donor bound excitons D^0X

TABLE III. Lifetimes of shallow and deeply bound excitons at 2 K. E_{loc} denotes the localization energy of the exciton, τ_{rise} the rise time, τ_1, $\tau_2 = \tau_{rec}$, and τ_{cap} the time constants for recombination and capture processes, and A_2/A_1 the amplitude ratio of the decay processes.

Exciton	Energy (eV)	E_{loc} (meV)	E_a (meV)	τ_{rise} (ps)	τ_1 (ps)	τ_2 (ps)	τ_{cap} (ps)	A_2/A_1
I_4	3.3628	13.1	13		230	570	165	0.33
I_6	3.3608	15.1	15		320	860	235	0.56
I_8	3.3598	16.1	16		375	1060	275	1.01
I_9	3.3567	19.2	19	200		1350		
Y_1	3.3363	39.6	12		185			
Y_0	3.3328	43.1	12		210			

via the capturing of free electrons by the ionized D^+ donors[83] which might contribute to the observed rise time. This charge transfer process from ionized to neutral bound exciton centers related to the same impurity is also demonstrated by excitation resonances in PLE measurements.[42,77]

The measured lifetimes of the various bound exciton transitions are plotted as function of the localization energy in Fig. 12(b). Apparently, both time constants of the shallow bound excitons I_4 to I_9 are proportional to $E_{\mathrm{loc}}^{3/2}$ whereby the τ_1 lifetimes are in good agreement with earlier studies by Heitz *et al.*[86] The observed relation for the shallow bound excitons can be explained by the model of Rashba and Gurgenishvili.[82] It is well known that the radiative lifetime is inversely proportional to the oscillator strength[87,88] with

$$\tau = \frac{ne^2\omega^2}{2\pi\epsilon_0 m_0 c^3 f}, \tag{4}$$

where f is the oscillator strength of the optical transition, ω is its frequency, n is the refractive index, and the other symbols have their usual meaning. According to Rashba and Gurgenishvili,[82,89] the oscillator strength of the bound excitons is proportional to the volume of the region occupied by the electron-hole complex where coherent oscillations of the electron polarization occur. In the case of an exciton which is weakly bound to the neutral donor center as a whole quasiparticle (i.e., for $E_{\mathrm{loc}} \ll E_{\mathrm{ex}}$), the radius of this region is determined by the localization energy as $a_{BE} \propto 1/\sqrt{E_{\mathrm{loc}}}$, where E_{ex} is the binding energy of the electron and hole in the exciton and a_{BE} is the Bohr radius of the bound exciton. Consequently, the radiative lifetime τ is proportional to the localization energy

$$\tau \propto 1/f \propto 1/a_{BE}^3 \propto E_{\mathrm{loc}}^{3/2}. \tag{5}$$

Despite the fact that this model is sufficient for a qualitative analysis, it should be noted that many contributions are neglected such as the correlation effects as pointed out by Sanders and Chang.[90] A corresponding effect is observed in confined potentials such as quantum wells and quantum dots. As the size of the nanostructure is reduced, the coherence volume of the exciton is also reduced leading to a decreasing oscillator strength and an increasing radiative lifetime.[91–93]

The fact that the observed recombination time $\tau_{\mathrm{rec}} = \tau_2$ scales with $E_{\mathrm{loc}}^{3/2}$ as expected for the radiative lifetime τ indicates that τ_{rec} is mostly determined by the radiative processes as was also pointed out by Heitz *et al.*[86] The same relation between time constants and localization energies is valid for the short lifetime τ_1 and therefore also for the recapture process of excitons to deep traps (τ_{cap}). This can be explained within the same model considering that the probability for an exciton to be detached from the shallow donor and to be recaptured to deeper traps is proportional to the overlap between the localized exciton wave function and the trap region and, therefore, to the localization volume $a_{BE}^3 \propto E_{\mathrm{loc}}^{-3/2}$. Furthermore, this explains the observed increase of the amplitude ratio A_2/A_1 with increasing localization energy (see Table III).

Returning to the time constants of the Y lines in Fig. 12(b), it is apparent that these transitions strongly violate the discussed relation of the shallow bound excitons between localization energy and recombination dynamics. Despite the large localization energy of the deeply bound excitons, similar lifetimes compared to the shallow bound exciton I_4 are observed. This discrepancy reminds of the unusually small thermal activation energies, Huang-Rhys parameters, and TES splittings of the Y lines with regard to their localization energy. Based on the lifetimes of the shallow bound excitons τ_1, the observed lifetimes of the Y lines would correlate to a binding energy of 12.0–12.7 meV. This value is in excellent agreement with the determined thermal activation energy $E_a = 12 \pm 2$ meV for these lines by temperature dependent PL measurements. The short lifetimes of the deeply bound excitons are not surprising since the condition $E_{\mathrm{loc}} \ll E_{\mathrm{ex}}$ is not satisfied anymore and, as discussed before, the exciton is not bound as a whole quasi-particle at these centers. In this model, the lowest thermal activation energy E_a corresponds to the detachment of one of the particles forming the exciton. The coherence volume of the exciton is then determined by the largest orbit and hence by E_a instead of E_{loc}.

H. Uniaxial compression

The application of pressure is a powerful tool to elucidate the elastic and electronic properties of semiconductors. In ZnO, hydrostatic pressure was widely used to study the phase transition from the wurtzite to the rocksalt structure[94,95] as well as a variety of phonon related parameters such as the Grüneisen parameters and the pressure dependence of the Born effective charge.[96,97] In addition, the phonon deformation potentials[98] and electronic deformation potentials[99] are usually determined by Raman spectroscopy and PL as function of uniaxial pressure. The application of uniaxial pressure leads to a deformation of the hexagonal lattice which enables the controlled variation of the c/a lattice ratio. In a wurtzite semiconductor with the space group C_{6v}^4, a reduction of symmetry is given for any uniaxial pressure direction which is not parallel to the c axis. The lifting of degeneracy caused by this symmetry reduction leads to a splitting of the optical transition lines. For pressure parallel to the c axis ($\boldsymbol{P} \| \boldsymbol{c}$), only a shift of the exciton energy levels occurs as the symmetry is unchanged. In this section, uniaxial pressure parallel to the c axis of the ZnO crystals is applied to clarify if the previously observed differences between shallow bound excitons and deeply bound excitons also manifest themselves in their pressure coefficients.

Figure 13 displays the PL spectra of the Cermet substrate in the range of the TES and Y transitions as function of uniaxial pressure at $T = 2$ K. In the depicted spectral range, the lines Y_0, Y_1, and Y_2/I_{12} are visible. With increasing pressure $\boldsymbol{P} \| \boldsymbol{c}$, all lines exhibit a shift toward higher energies. This shift is caused by the compressive strain $\varepsilon_{zz} < 0$ along the c axis due to the external pressure and the respective biaxial expansion $\varepsilon_{xx} = \varepsilon_{yy} > 0$ in the plane perpendicular to the c axis. The energetic position of each line is carefully determined and plotted as function of the pressure onto the sample in Fig. 14(b). From the linear fits of these values, the uniaxial pressure coefficients of the observed bound exciton transitions are determined [Fig. 14(a)] and listed in Table IV. For the shallow bound excitons, pressure coefficients between 2.79 meV/GPa (I_4) and 3.37 meV/GPa (I_9) are derived. By

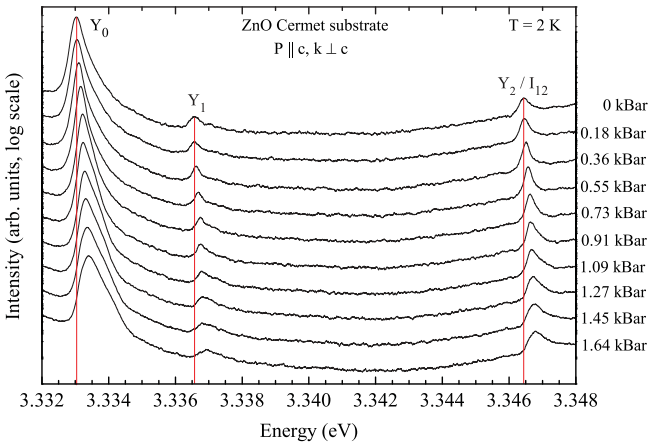

FIG. 13. (Color online) PL spectra of the Cermet substrate as function of external uniaxial pressure $\boldsymbol{P}\|\boldsymbol{c}$ between 0 kBar and 1.64 kBar in the range of the deeply bound exciton lines at $T = 2$ K. Vertical red lines mark the peak energies without external pressure.

contrast, the Y_0, Y_1, and Y_2/I_{12} bound excitons show a significantly smaller pressure dependence upon uniaxial compression with values around 2.1 meV/GPa. Based on the comparable pressure coefficients of Y_0, Y_1, and Y_2/I_{12}, these three lines are attributed to the same group of deeply bound exciton transitions. If the Y_2 belongs to the "shallow" bound excitons (I lines), a significantly higher uniaxial pressure coefficient would be expected which scales with the localization energy E_{loc} or rather the associated donor binding energy E_D. However, this is obviously not the case. To express this difference also in the name of the exciton recombination line, it is suggested to label the 3.3465 eV transition in ZnO Y_2 instead of I_{12}. It should be noted that the Y_2 line was not clearly visible in the ZnO substrate prior to the uniaxial pressure measurements (see also Fig. 2). Therefore, it is likely that the Y_2/I_{12} emission line originates from structural defects which were created due to the application of uniaxial pressure.

As can be seen from Fig. 14(a), all bound exciton lines display a smaller energy shift as function of uniaxial pressure than

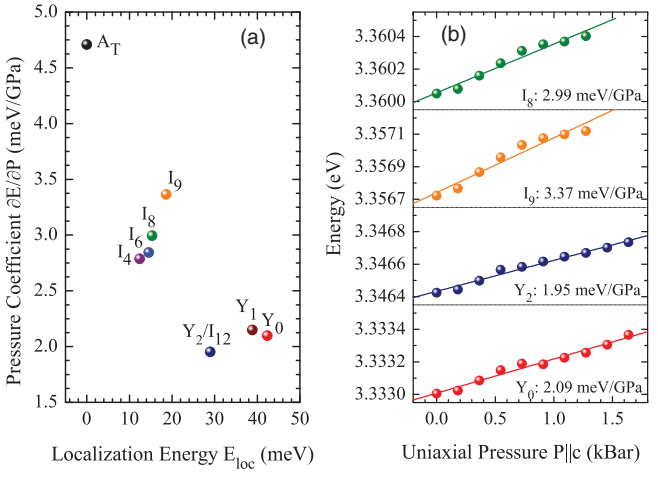

FIG. 14. (Color online) (a) Pressure coefficients for shallow and deeply bound excitons, (b) shifting behavior of the I_8, I_9, Y_2/I_{12}, and Y_0 lines as function of applied uniaxial pressure.

TABLE IV. Uniaxial pressure coefficients of free, shallow, and deeply bound excitons for pressure $\boldsymbol{P}\|\boldsymbol{c}$ at 2 K. E_{loc} denotes the localization energy of the exciton, E_a the thermal activation energy, $\partial E/\partial P$ the uniaxial pressure coefficient in absolute energies and $\partial E_{\mathrm{loc}}/\partial P$ the pressure coefficient in localization energies.

Exciton	Energy E (eV)	E_{loc} (meV)	E_a (meV)	$\partial E/\partial P$ (meV/GPa)	$\partial E_{\mathrm{loc}}/\partial P$ (meV/GPa)
FX(A_T)	3.3759			4.71	
I_4	3.3628	13.1	13	2.79	1.92
I_6	3.3608	15.1	15	2.84	1.87
I_8	3.3598	16.1	16	2.99	1.72
I_9	3.3567	19.2	19	3.37	1.34
Y_2/I_{12}	3.3465	29.4		1.95	2.76
Y_1	3.3363	39.6	12	2.15	2.56
Y_0	3.3328	43.1	12	2.09	2.62

the free exciton line FX(A_T). Thus, the localization energy of all bound excitons increases upon uniaxial compression. For the shallow bound excitons (I_i), the influence of the pressure on the localization energy is larger in the case of shallow centers and smaller for deeper centers. In other words, the absolute pressure coefficients of the bound excitons are increasing with increasing localization energy. The increase of the localization energy with uniaxial pressure for the shallow bound excitons and its dependence on the initial localization energy can be explained within the model of excitons localized as whole quasiparticles at the shallow impurity centers.[100] However, the largest effect of the uniaxial compression in relation to the pressure dependence of the free exciton (smallest absolute pressure coefficient) is found for the Y_0, Y_1, and Y_2/I_{12} lines (Table IV) which indicates a distinctly different structure of the Y defect cores in comparison to the shallow bound excitons. Possible mechanisms of the additional stress effect on the deeply bound exciton complexes are discussed in Sec. IV.

I. Spatial distribution of defect centers

To study the structure and distribution of the defects related to the emission of the different bound exciton lines, monochromatic cathodoluminescence images were recorded at 6 K. Figure 15 shows CL images at two different sample positions at the energy of the Y_0 emission line in comparison to the adjacent TES emission of the I_4 bound exciton. Clearly, the two emission peaks originate from distinctly different spatial areas. For the TES luminescence, a mostly uniform distribution in the undistorted areas of the surface is observed. In contrast, the Y lines show the strongest intensity in the direct vicinity of linear cracks and from within the branches of hexagonal star-like defects. The intense Y_0 luminescence originating from areas with strong local distortions in the crystal lattice confirms that these lines are related to extended structural defects. Confocal micro-PL scans further indicate a weaker intensity dependence of the Y lines on the focus position compared to the I lines. In the case of surface localized states, the opposite behavior would be expected. Another argument against surface related defects is given by the absence of these lines in nanostructures with dimensions below 100 nm as they exhibit an increased surface to volume ratio.[15,19,21,101]

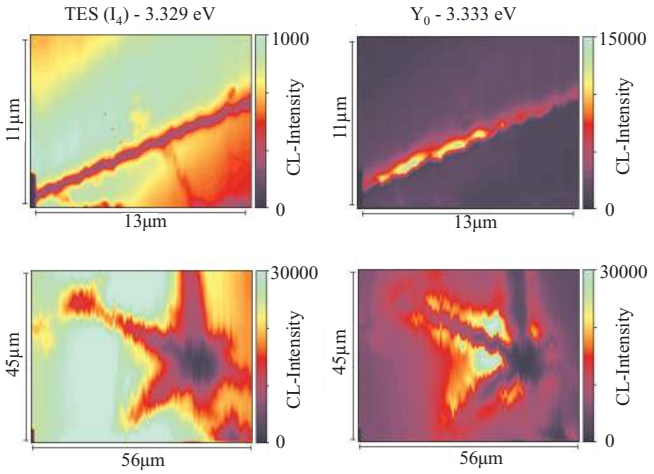

FIG. 15. (Color online) Monochromatic CL images in the vicinity of structural defects in ZnO at the spectral positions of the TES(I_4) (left) and Y_0 (right) emission lines for an acceleration voltage of 15 kV at $T = 6$ K. Top: linear crack, bottom: hexagonal star-like defect.

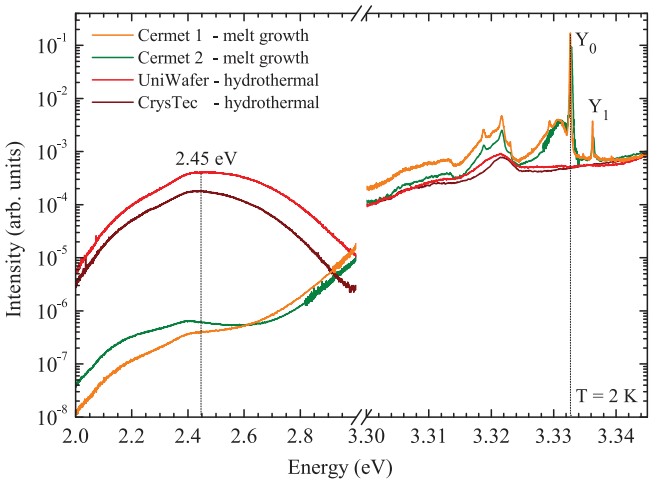

FIG. 16. (Color online) Photoluminescence spectra of different ZnO substrates in the range of the green luminescence band and Y transitions at $T = 2$ K. Strong Y lines are observed in samples with weak green luminescence bands (Cermet, melt growth). Samples with strong emission bands around 2.45 eV do not show any defect bound exciton transitions (CrysTec and UniWafer, hydrothermal growth). All spectra are normalized to the dominant bound exciton luminescence.

Thus, it is concluded that the Y lines originate from defect centers such as dislocations which are not surface related. This is similar to the basal plane stacking faults giving rise to the 3.31 eV transition as discussed by Schirra *et al.*[12] A possible explanation for the smaller focal dependency could be given by the larger excitation volume of these lines due to reabsorption of light from bound exciton emissions. The efficient capture of charge carriers to these centers as well as the significantly smaller absorption coefficient at the energy of deeper bound exciton emission lines in comparison to the above band edge laser excitation might lead to an excitation of defect centers well beyond the penetration depth of the laser light with wavelengths of 266 and 325 nm. Therefore, a reduced dependence of the focal position in the samples should be expected.

J. Defect bound excitons and green luminescence

Following the assignment of the Y lines to defect bound excitons at extended structural defects, the question arises if the appearance of these transitions goes along with other defect related luminescence bands. One of the most prominent candidates is this context is the green luminescence band in ZnO. To investigate a possible correlation between these luminescence features, we have studied the luminescence intensity of different substrates in a large dynamic range. Figure 16 shows the luminescence spectra of four different ZnO substrates which were grown using the melt growth technique (Cermet) or the hydrothermal growth method (UniWafer, CrysTec) in the region of the Y lines and the green luminescence band. The comparison of the PL spectra of the different substrates reveals indeed a connection between the intensity of the green luminescence band and the defect bound exciton lines in these samples: The melt grown samples exhibit pronounced Y_0 and Y_1 emission lines, but a very weak green luminescence band. In contrast, the hydrothermally grown samples show no Y transitions, however, a strong green luminescence band is observed whose intensity is about three orders of magnitude larger than in the melt grown samples. Based on these observations, an anticorrelation of these two luminescence features is conceivable. Thereby, the Y lines would constitute an alternative recombination channel to the green luminescence band. Since the green luminescence originates (in the absence of copper) from mobile intrinsic point defects such as zinc or oxygen vacancies,[56,102,103] it is possible that the presence of extended structural defects (Y centers) is accompanied by a reduced amount of native point defects. In this case, it could be argued that these point defects accumulate at dislocations in samples with pronounced Y emission lines which results in an reduction of the 2.45 eV band and an intensity increase of the luminescence lines of excitons bound to extended structural defects. Following this line of argumentation, the melt growth technique would favor the presence of extended structural defects in comparison to the hydrothermal growth, but, in turn, lead to a reduction of the green luminescence band due to native point defects. Further research is required to obtain a deeper understanding about the suggested anticorrelation between the luminescence features of point defects and extended structural defects.

K. Defect bound excitons in other compound semiconductors

Dean *et al.* first reported luminescence peaks in ZnSe labeled Y and Z which were attributed to localized recombinations within extended defects, involving a noncentral force electronic system.[75,104] In particular, a strong intensity of these lines was observed in the vicinity of heteroepitaxial interfaces in CVD grown samples as well as cut bulk samples. Similar observations of excitonic recombinations at structural defects have also been reported in many other II–VI and III–V semiconductors such as ZnTe, CdTe, ZnS, CdS, GaN, and GaP.[41,46,105–107] Naumov *et al.*[105] discovered that the intensity of Y line emissions in ZnTe epilayers is a function of the

lattice mismatch between layer and substrate and concluded that the observed luminescence is related to recombinations of excitons bound to extended structural defects which should be represented by misfit dislocations. Similar transition lines were also found in CdTe which were attributed to excitons bound to structural defects such as twins, dislocations, or stacking faults.[106] In addition, Hoffmann *et al.*[107] and Gutowski *et al.*[46] performed monochromatic cathodoluminescence and magnetooptical Zeeman studies on CdS specimen, respectively. Several luminescence lines were attributed to defect bound excitons associated with screw dislocations. The Zeeman splitting of these lines was found to be rather isotropic in contradiction to the usual anisotropy for recombinations at point defects under the influence of the local crystal field. It was concluded that the observed emission lines are related to deep excitons bound to dislocations, from which two lines exhibited an ionized-donor-complex-like behavior. The presence of emission lines related to defect bound excitons in such a variety of different compound semiconductors impressively demonstrates the relevance of extended structural defects and strongly suggests the presence of extended defect bound exciton complexes with similar properties in ZnO.

IV. DISCUSSION AND CONCLUSION

So far, we have presented a variety of different experimental results which showed distinctly different properties for the Y lines in comparison to the I lines. The properties of the shallow bound excitons (I lines) could be well explained for bound excitons localized as whole quasiparticles at shallow donors. Within this section, we compare these results and discuss possible qualitative models for the Y lines based on the experimental observations. The main results are briefly summarized for each section as basis for the following discussion.

(1) The Y lines are related to excitonic recombinations from a complex consisting of two electrons and one hole with Γ_7 symmetry (Sec. III B). This configuration is similar to excitons bound to neutral shallow donors. The Y-line centers act as additional donors in ZnO.

(2) The lowest activation potential E_a (12 meV) for the Y centers is significantly smaller than the localization energy E_{loc} (about 40 meV) and the exciton binding energy E_{ex} (60 meV). Therefore, the thermal activation energy E_a does not correspond to the detachment of the exciton as a whole quasiparticle indicating that one of the particles (electron) forming the exciton is bound more deeply to the defect core while the second particle (hole) is weakly bound. The localization energy of the exciton in such a complex is given by

$$E_{\mathrm{loc}} = (E_{2e} - E_e) + E_h - E_{\mathrm{ex}}. \tag{6}$$

Here, E_{2e} is the binding energy of two electrons at the defect core, E_e is the binding energy of one ground state electron, and E_h is the binding energy of the hole at the complex. For $E_h \ll E_{2e} - E_e$, the thermal activation energy of such a complex is given by $E_a \approx E_h$. This behavior is different from excitons bound to neutral shallow donors where the thermal activation energy is equal to the binding energy of the whole exciton at an impurity center with $E_a = E_{\mathrm{loc}}$.

(3) One possible defect model explaining these results could consist of a doubly charged donor core D^{2+}. Such a center may possess one electron in the ground state and bind a second electron and a hole to form a bound exciton complex. However, in the case of a doubly charged donor core, the binding energy of the ground state electron E_e in the effective mass approximations equals $4E_B$, where E_B is the binding energy of a single charged effective mass donor. Thus, a greatly increased energy spacing between the exciton and its two electron satellite would be expected which is in contradiction to the energy of the observed TES transitions (see Fig. 9 in Sec. III D). Consequently, the potential of the defect core should be strong enough to tightly bind the second electron while the binding energy of the first electron is not large. This is only possible if the electron-electron repulsion in the complex is reduced which occurs in the case of an extended defect core. Such an extended defect core might be composed of two or more donor ions, created by several short-range potentials, or be similar to the dislocation loops described by Dean.[75] It can be characterized by a structural parameter R or alternatively by the strain field induced by the dislocation. A theoretical description for dislocation bound excitons in II-VI semiconductors was developed by Rebane, Schreter, and Steeds,[108–111] which assumes that the exciton forming carriers are bound to a dislocation by its strain field.

(4) The model of the extended defect core may also account for the very small Huang-Rhys parameter S which is observed for these lines.[75] Comparable values for the Huang-Rhys factor of defect bound excitons were reported in other compound semiconductors such as ZnSe and ZnTe. In ZnSe, the Huang-Rhys factor of similar structural defect bound exciton lines Y and Z varies between $S = 0.2$ and 0.02, respectively.[75,112] In ZnTe, Naumov *et al.*[105] reported Huang-Rhys values for the defect bound excitons Y_1 and Y_2 of $S < 0.01$ and $S = 0.2$, respectively. These values are about one order of magnitude smaller than predicted for point defects with the same localization energy in ZnTe (Ref. 75). In agreement with these materials, the derived Huang-Rhys factor $S = 0.004 \pm 0.002$ for the Y_0 line in ZnO is about one order of magnitude smaller than those of the shallow impurity bound excitons in ZnO.

(5) As a simple example of the extended defect model, we consider a double donor complex consisting of one neutral and one singly ionized donor. An exciton bound to this complex can contribute one electron to the ionized donor resulting in two tightly bound electrons at two singly positively charged donors and one weakly bound hole. The spins of the electrons will be oriented antiparallel to each other. This model is in agreement with the observed linear line splitting in a magnetic field since only one unpaired charge carrier is present which is comparable to a simple neutral donor bound exciton. Due to the weak binding energy of the unpaired particle, the hole can be easily detached from the complex which could explain the small thermal activation energy $E_a \approx E_h < E_{\mathrm{loc}}$. A schematic drawing of such a complex is shown in Fig. 17(a). The distance R between the D^+ ions in the defect core characterizes the spatial extension of the structural defect and should be greater than twice the Bohr radius a_B of the effective mass donor. In

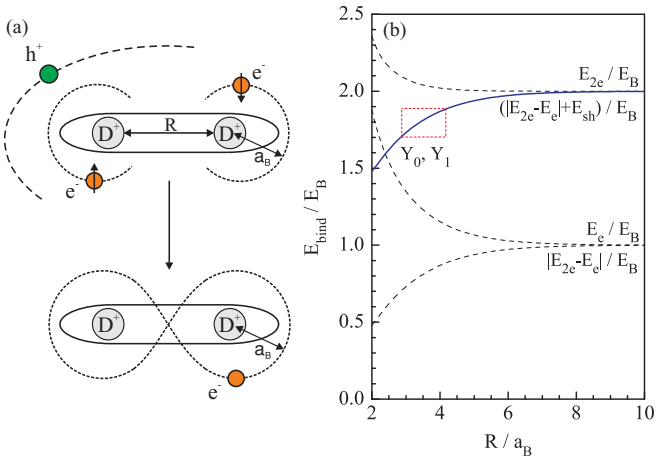

FIG. 17. (Color online) (a) Schematic picture of an extended defect bound exciton complex. The defect core consists of two singly charged D^+ ions separated by a distance $R > 2a_B$, where a_B is the Bohr radius of the effective mass donor. The ground state of the complex is represented by one electron bound to the defect core. In the excited state, two electrons with antiparallel spins are strongly bound to the defect core while the hole is weakly bound to the complex. (b) Dependency of the binding energy of the ground state electron E_e, of two electrons in the excited state E_{2e}, and of the second electron $|E_{2e} - E_e|$ on the distance R between ions. The energy is measured in the effective mass Bohr energy E_B. The solid line shows the dependence of the second electron binding energy on R taking a short-range potential correction of the order of E_B into account. The red box marks the characteristic region of an increasing binding energy for the Y centers.

this case the asymptotic expressions can be obtained for the binding energy of one electron E_e and two electrons E_{2e} bound to the D^+-D^+ defect core.[113,114]

Within this qualitative defect model, the binding energies of one electron E_e, two electrons E_{2e}, and the second electron $E_{2e} - E_e$ can be determined as function of the distance R which are shown by dashed lines in Fig. 17(b). For large distances R, the ions are independent of the electron configuration and the one electron and two electron energies converge to the Bohr effective mass energy E_B of about 50 meV (Ref. 27): $E_e \to E_B$ and $E_{2e} \to 2E_B$ (see Fig. 17(b)). With decreasing R, the attraction of the second ion leads to an increase of E_e and E_{2e}. However, the electron-electron repulsion reduces the two electron binding energy E_{2e} and, hence, the binding energy of the second electron. The resulting binding energy of the second electron $E_{2e} - E_e$, which is calculated in the effective mass approximation with the Coulomb potential of the ions, is too small to result in a localization energy of the complex larger than the thermal activation energy E_a. In fact, the short-range potential corrections for both D^+ ions should be taken into account. Assuming the short-range potential correction energy $E_{\rm sh}$ to be the same for both ions, one has to add $E_{\rm sh}$ to E_e to obtain the binding energy of the first electron, and $2E_{\rm sh}$ to E_{2e} to obtain the energy of two electrons. As the result, the binding energy of the second electron is given by $E_{2e} - E_e + E_{\rm sh}$. For the case that the energy of the short-range potential correction equals the Bohr effective mass energy $E_{\rm sh} = E_B$, the dependence of the binding energy of the second electron on the ion distance R is shown in Fig. 17(b) by the solid line. From a binding energy of the free exciton of $E_{\rm ex} = 60$ meV, the values of $E_{2e} - E_e$ are calculated to about 90 meV for the Y_0 line and 86 meV for the Y_1 line. These values are obtained with an thermal activation energy of $E_a = 12$ meV and localization energies of $E_{\rm loc} = 43.1$ and 39.6 meV, respectively. With $E_B \approx 50$ meV (Ref. 27) and $E_{\rm sh} = E_B$, the Y lines should be related to an extended defect complex with a distance between the D^+ ions of about 3.5 to 4.0 a_B. Following these estimations the resulting binding energy E_e of the ground state electron to the D^+-D^+ defect core is about 110 to 115 meV. This value is much smaller than the expected value of 200 to 250 meV for the ground state electron state at the D^{2+} core. However, it is too large to account for the observed TES separation of about 65 meV (see Fig. 9 in Sec. III D) if one assumes that this transition corresponds to the $2S/2P$ excited state of the electron. We therefore conclude that the first excited state of the single electron bound to the D^+-D^+ defect core should have a binding energy of about 45–50 meV. It should be noted that the derived values for the extent of the defect and the binding energies are valid within the suggested illustrative description of the defect complex. However, while the linewidth is very narrow in the investigated samples and thus suggests a uniform size of the defect complex, a larger width of the Y lines is sometimes reported in the literature which could be related to a distribution of defect complexes with different extents. These considerations reveal the limitations of the discussed illustrative model and advanced theoretical calculations are required to describe the size distribution and extents of the defects with greater precision. In any case, however, an extended structural defect is required to explain the presented experimental data.

(6) The study of the energetic shift of the different exciton lines as function of temperature in Fig. 5 has shown that an increasing temperature results in a decreasing localization energy of the shallow bound excitons while the localization energy of the Y lines increases (Sec. III C). The decrease of the localization energy for the shallow bound excitons can be explained by the screening of the impurity potential by free carries which increase with temperature. By contrast, the increase of the localization energy for the deeply bound excitons should be related to the effect of the temperature on the structural parameter R of the defect core or the strain field of the dislocation.

(7) A comparison of the recombination dynamics between I lines and Y lines reveals short and monoexponential lifetimes in the case of the defect center related excitons and longer biexponential time constants for the I lines (see Fig. 12 and Table III in Sec. III G). While the lifetimes of the shallow bound excitons increase as function of the localization energy as described by the model of Rashba and Gurgenishvili,[82] the lifetimes of the defect bound excitons do not scale with the large localization energies $E_{\rm loc}$ of these centers, but rather with the small thermal activation energies E_a. This is well explained by the presented model since the thermal activation energy $E_a \approx E_h$ corresponds to the detachment of the weakly bound hole. The radius of its orbit $a_h \propto 1/\sqrt{E_a}$ determines the coherence region occupied by the exciton and thus the radiative lifetime. In addition, nonradiative decay channels for these deep centers related to the activation and recapture of

the shallow bound hole might contribute to the observed short lifetimes. These additional decay channels should not saturate resulting in the observed monoexponential decay characteristic of the Y lines. A rising time is not observed for the Y lines within the experimental time resolution of about 20 ps which indicates a very fast formation of the complexes. This could be supported by the presence of an additional capture process of charge carriers. According to the presented model, these bound exciton complexes can be created not only by the capture of free exciton at the ionized $D^+ - D^0$ defect, but also by the capture of a hole to the neutral $D^0 - D^0$ defect. The measured decay dynamics of the Y lines in ZnO are in agreement with the short and monoexponential decay of defect bound excitons in ZnSe reported by Dean.[75]

(8) The uniaxial compression along the c axis results in increasing localization energies of the shallow impurity bound excitons (I lines) and defect center bound excitons (Y lines) as discussed in Sec. III H (see Fig. 14). The effect of the uniaxial stress on the localization energies was observed to be larger for the Y lines than for the I lines. Within the presented defect model, this difference should be caused by an additional effect of the strain on the internal structural parameter R of the defect core. Assuming the defect core is extended in the plain perpendicular to the c axis, the uniaxial compression parallel to the c axis would lead to an increase of the structural parameter R of the defect core (or of the dislocation strain field) which is caused by the biaxial expansion $\varepsilon_{xx} = \varepsilon_{yy} > 0$ of the lattice in the plain perpendicular to the c axis. In turn, the larger distance R results in a reduced effect of the electron-electron repulsion and hence in an increase of the localization energy E_{loc} with increasing uniaxial pressure. This relation is visualized by the dashed red rectangle in Fig. 17(b) which marks a characteristic region of increasing binding energy of the second electron $E_{2e} - E_e$ as a function of R for the Y centers in the considered defect model. Taking Eq. (6) into account, it is apparent that the increase of $E_{2e} - E_e$ is equivalent to an increase of E_{loc}. While the tendency is correct, the increase rate of the binding energy $E_{2e} - E_e$ as function of R, which is predicted by the calculations shown in Fig. 17(b), is too small in comparison to the experimentally observed pressure coefficients for the localization energy. A larger rate can be obtained if one assumes the presence of several short-range potential wells between the ionized ions in the defect core. For such a model, additional theoretical calculations are required.

V. SUMMARY

In conclusion, a comprehensive study of the origin and properties of deeply bound exciton lines was conducted and the results were compared to shallow impurity bound excitons. Based on a variety of experimental results, it was shown that the Y_0 (3.3328 eV), Y_1 (3.3363 eV), and Y_2 (3.3465 eV) lines originate from the radiative recombination of excitons bound to extended structural defects. These defect complexes introduce additional donor states which may reduce or hinder p conductivity in acceptor doped ZnO. All three lines cannot be described within the effective mass like model for shallow donor states. Rather, a model of deeply bound excitons with one weakly bound charge carrier was developed and discussed. A small thermal activation energy of about 12 meV is derived from temperature dependent PL spectra in contrast to the more than three times larger localization energy of these excitons. An additional doublet structure around 3.270 eV is exclusively observed in samples which exhibit the Y_0 emission line and is identified as its two electron satellite transitions. The energy spacing of these TES lines as well as the Huang-Rhys parameter $S = 0.004 \pm 0.002$ of the Y_0 line were found to be exceptionally small. The recombination dynamics of the different exciton transitions exhibit striking differences between the shallow impurity and deep defect bound excitons. While the lifetime of the shallow bound excitons increases as function of the localization energy between 570 ps and 1.35 ns, significantly shorter lifetimes of about 200 ps are determined for the defect bound excitons. A comparable tendency is observed for the uniaxial pressure coefficients ($P \| c$) of the different bound excitons with values of around 2 meV/GPa for the defect bound excitons between 3.33 and 3.35 eV and 2.8 to 3.2 meV/GPa for the shallow donor bound exciton I_4 to I_9. In addition, monochromatic CL images show that the Y lines originate from microscopically localized structures such as line defects and the areas in between the branches of hexagonal star-like defects. Furthermore, an anticorrelation between the green luminescence band caused by point defects and the Y lines due to extended defects is observed. The different experimental results can be explained within the presented qualitative model of excitons bound to extended structural defects. Several properties of these exciton complexes such as their short monoexponential decay dynamics and weak exciton-phonon coupling are found to be in excellent agreement with reports of defect and dislocation bound excitons in other III–V and II–VI compound semiconductors.

ACKNOWLEDGMENTS

Parts of this work were supported by the DFG within SFB 787. M.R.W. acknowledges support of the cluster of excellence "Unifying Concepts in Catalysis–UniCat." A.V.R. acknowledges support from the RFFI Grant No. 09-0201296-a.

*markus.wagner@tu-berlin.de

[1] M. Zamfirescu, A. Kavokin, B. Gil, G. Malpuech, and M. Kaliteevski, Phys. Rev. B **65**, 161205(R) (2002).

[2] T. Gruber, C. Kirchner, R. Kling, F. Reuss, and A. Waag, Appl. Phys. Lett. **84**, 5359 (2004).

[3] E. Tomzig and R. Helbig, J. Lumin. **14**, 403 (1976).

[4] A. Schildknecht, R. Sauer, and K. Thonke, Physica B **340**, 205 (2003).

[5] R. Sauer and K. Thonke, in *Optics of Semiconductors and Their Nanostructures*, edited by H. Kalt and M. Hetterich (Springer, New York, 2004), p. 73.

[6] M. R. Wagner, P. Zimmer, A. Hoffmann, and C. Thomsen, Phys. Stat. Sol. RRL **1**, 169 (2007).

[7]D. C. Look, D. C. Reynolds, C. W. Litton, R. L. Jones, D. B. Eason, and G. Cantwell, Appl. Phys. Lett. **81**, 1830 (2002).
[8]M. R. Wagner, U. Haboeck, P. Zimmer, A. Hoffmann, S. Lautenschläger, C. Neumann, J. Sann, and B. K. Meyer, Proceedings of SPIE **6474**, 64740X (2007).
[9]S. Lautenschläger, S. Eisermann, B. K. Meyer, G. Callsen, M. R. Wagner, and A. Hoffmann, Phys. Stat. Sol. RRL **3**, 16 (2009).
[10]H. Kato, M. Sano, K. Miyamoto, and T. Yao, Jpn. J. Appl. Phys. **42**, 2241 (2003).
[11]H. Shibata, M. Watanabe, M. Sakai, K. Oka, P. Fons, K. Iwata, A. Yamada, K. Matsubara, K. Sakurai, H. Tampo, K. Nakahara, and S. Niki, Phys. Status Solidi C **1**, 872 (2004).
[12]M. Schirra, R. Schneider, A. Reiser, G. M. Prinz, M. Feneberg, J. Biskupek, U. Kaiser, C. E. Krill, K. Thonke, and R. Sauer, Phys. Rev. B **77**, 125215 (2008).
[13]I. C. Robin, P. Marotel, A. H. El-Shaer, V. Petukhov, A. Bakin, A. Waag, M. Lafossas, J. Garcia, M. Rosina, A. Ribeaud, S. Brochen, P. Ferret, and G. Feuillet, J. Cryst. Growth **311**, 2172 (2009).
[14]T. Hirai, Y. Harada, S. Hashimoto, N. Ohno, and T. Itoh, J. Lumin. **113**, 115 (2005).
[15]J. Fallert, R. J. B. Dietz, M. Hauser, F. Stelzl, C. Klingshirn, and H. Kalt, J. Lumin. **129**, 1685 (2009).
[16]S. Polarz, A. Orlov, A. Hoffmann, M. R. Wagner, C. Rauch, R. Kirste, W. Gehlhoff, Y. Aksu, M. Driess, M. W. E. van den Berg, and M. Lehmann, Chem. Mater. **21**, 3889 (2009).
[17]C. Rauch, W. Gehlhoff, M. R. Wagner, E. Malguth, G. Callsen, R. Kirste, B. Salameh, A. Hoffmann, S. Polarz, Y. Aksu, and M. Driess, J. Appl. Phys. **107**, 024311 (2010).
[18]R. Kirste, Y. Aksu, M. R. Wagner, S. Khachadorian, S. Jana, M. Driess, C. Thomsen, and A. Hoffmann, Chem. Phys. Chem. **12**, 1189 (2011).
[19]D. Stichtenoth, C. Ronning, T. Niermann, L. Wischmeier, T. Voss, C.-J. Chien, P.-C. Chang, and J. G. Lu, Nanotechnology **18**, 435701 (2007).
[20]M. Lange, J. Zippel, G. Benndorf, C. Czekalla, H. Hochmuth, M. Lorenz, and M. Grundmann, J. Vac. Sci. Technol. B **27**, 1741 (2009).
[21]M. Lorenz, J. Lenzner, E. M. Kaidashev, H. Hochmuth, and M. Grundmann, Ann. Phys. (Leipzig) **13**, 39 (2004).
[22]J. S. Reparaz, F. Güell, M. R. Wagner, A. Hoffmann, A. Cornet, and J. R. Morante, Appl. Phys. Lett. **96**, 053105 (2010).
[23]K. Johnston, M. O. Henry, D. McCabe, E. McGlynn, M. Dietrich, E. Alves, and M. Xia, Phys. Rev. B **73**, 165212 (2006).
[24]B. Wang, M. J. Callahan, L. O. Bouthillette, and M. J. S. C. Xu, J. Cryst. Growth **287**, 381 (2006).
[25]H. Tampo, H. Shibata, P. Fons, A. Yamada, K. Matsubara, K. Iwata, K. Tamura, H. Takasu, and S. Niki, J. Cryst. Growth **278**, 268 (2005).
[26]H. Alves, D. Pfisterer, A. Zeuner, T. Riemann, J. Christen, D. M. Hofmann, and B. K. Meyer, Opt. Mater. **23**, 33 (2003).
[27]B. K. Meyer, H. Alves, D. M. Hofmann, W. Kriegseis, D. Forster, F. Bertram, J. Christen, A. Hoffmann, M. Straßburg, M. Dworzak, U. Haboeck, and A. V. Rodina, Phys. Status Solidi B **241**, 231 (2004).
[28]K. Thonke, T. Gruber, N. Teofilov, R. Schönfelder, A. Waag, and R. Sauer, Physica B **308**, 945 (2001).
[29]D. C. Look, C. Coskun, B. Claflin, and G. C. Farlow, Physica B **340**, 32 (2003).
[30]S. F. Chichibu, T. Onuma, M. Kubato, A. Uedono, T. Sota, A. Tsukazaki, A. Ohtomo, and M. Kawasaki, J. Appl. Phys. **99**, 093505 (2006).
[31]K. Iwata, H. Tampo, A. Yamada, P. Fons, K. Matsubara, K. Sakurai, S. Ishizuka, and s. Nici, Appl. Surf. Sci. **244**, 504 (2005).
[32]M. R. Wagner, T. P. Bartel, R. Kirste, A. Hoffmann, J. Sann, S. Lautenschläger, B. K. Meyer, and C. Kisielowski, Phys. Rev. B **79**, 035307 (2009).
[33]T. Gruber, G. M. Kirchner, R. Kling, F. Reuss, W. Limmer, and A. Waag, J. Appl. Phys. **96**, 289 (2004).
[34]L. Wang and N. C. Giles, Appl. Phys. Lett. **84**, 3049 (2004).
[35]S. Heitsch, C. Bundesmann, G. Wagner, G. Zimmermann, A. Rahm, H. Hochmuth, G. Benndorf, H. Schmidt, M. Schubert, M. Lorenz, and M. Grundmann, Thin Solid Films **496**, 234 (2006).
[36]S. H. Park, T. Hanada, D. C. Oh, T. Minegishi, H. Goto, G. Fujimoto, J. S. Park, I. H. Im, J. H. Chang, M. W. Cho, T. Yao, and K. Inaba, Appl. Phys. Lett. **91**, 231904 (2007).
[37]C. Bekeny, T. Voss, B. Hilker, J. Gutowski, R. Hauschild, H. Kalt, B. Postels, A. Bakin, and A. Waag, J. Appl. Phys. **102**, 044908 (2007).
[38]B. K. Meyer, J. Sann, S. Lautenschläger, M. R. Wagner, and A. Hoffmann, Phys. Rev. B **76**, 184120 (2007).
[39]U. Özgür, Y. I. Alivov, C. Liu, A. Teke, M. A. Reshchikov, S. Doğan, Avrutin, S.-J. Cho, and H. Morkoç, J. Appl. Phys. **98**, 041301 (2005).
[40]D. W. Hamby, D. A. Lucca, and M. J. Klopfstein, J. Appl. Phys. **96**, 043504 (2005).
[41]S. Fischer, G. Steude, D. M. Hofmann, F. Kurth, F. Anders, M. Topf, B. K. Meyer, F. Bertram, M. Schmidt, J. Christen, L. Eckey, J. Holst, A. Hoffmann, B. Mensching, and B. Rauschenbach, J. Cryst. Growth **189**, 556 (1998).
[42]M. Brandt, H. von Wenckstern, G. Benndorf, M. Lange, C. P. Dietrich, C. Kranert, C. Sturm, R. Schmidt-Grund, H. Hochmuth, M. Lorenz, M. Grundmann, M. R. Wagner, M. Alic, C. Nenstiel, and A. Hoffmann, Phys. Rev. B **81**, 073306 (2010).
[43]Y. Ohno, H. Koizumi, T. Taishi, I. Yonenaga, K. Fujii, H. Goto, and T. Yao, J. Appl. Phys. **104**, 073515 (2008).
[44]M. R. Wagner, J.-H. Schulze, R. Kirste, M. Cobet, A. Hoffmann, C. Rauch, A. V. Rodina, B. K. Meyer, U. Röder, and K. Thonke, Phys. Rev. B **80**, 205203 (2009).
[45]A. V. Rodina, M. Strassburg, M. Dworzak, U. Haboeck, A. Hoffmann, A. Zeuner, H. R. Alves, D. M. Hofmann, and B. K. Meyer, Phys. Rev. B **69**, 125206 (2004).
[46]J. Gutowski and A. Hoffmann, Mater. Sci. Forum **38**, 1391 (1989).
[47]M. R. Wagner, H. W. Kunert, A. G. J. Machatine, A. Hoffmann, P. Niyongabo, J. Malherbe, and J. Barnas, Microelectron. J. **40**, 289 (2009).
[48]P. H. Kasai, Phys. Rev. **130**, 989 (1963).
[49]D. Block, A. Herve, and R. T. Cox, Phys. Rev. B **25**, 6049 (1982).
[50]D. M. Hofmann, A. Hofstaetter, F. Leiter, H. Zhou, F. Henecker, B. K. Meyer, S. B. Orlinskii, J. Schmidt, and P. G. Baranov, Phys. Rev. Lett. **88**, 045504 (2002).
[51]D. Galland and A. Herve, Phys. Lett. A **33**, 1 (1970).
[52]D. Galland and A. Herve, Solid State Commun. **14**, 953 (1974).
[53]L. S. Vlasenko and G. D. Watkins, Phys. Rev. B **72**, 035203 (2005).
[54]X. J. Wang, L. S. Vlasenko, S. J. Pearton, W. M. Chen, and I. A. Buyanova, J. Phys. D **42**, 175411 (2009).
[55]A. F. Kohan, G. Ceder, D. Morgan, and C. G. V. de Walle, Phys. Rev. B **61**, 15019 (2000).

[56] S. B. Zhang, S. H. Wei, and A. Zunger, Phys. Rev. B **63**, 075205 (2001).
[57] F. Tuomisto, V. Ranki, K. Saarinen, and D. C. Look, Phys. Rev. Lett. **91**, 205502 (2003).
[58] D. G. Thomas, J. Phys. Chem. Solids **15**, 86 (1960).
[59] Y. P. Varshni, Physica **34**, 149 (1967).
[60] A. Manoogian and J. C. Woolley, Can. J. Phys. **62**, 285 (1984).
[61] K. P. O'Donnell and X. Chen, Appl. Phys. Lett. **58**, 2924 (1991).
[62] R. Pässler, Phys. Status Solidi B **236**, 710 (2003).
[63] A. R. Hutson, J. Phys. Chem. Solids **8**, 467 (1959).
[64] L. Vina, S. Logothetidis, and M. Cardona, Phys. Rev. B **30**, 1979 (1984).
[65] J. Wang, G. Du, B. Zhao, X. Yang, Y. Zhang, Y. Ma, D. Liu, Y. Chang, H. Wang, H. Yang, and S. Yang, J. Cryst. Growth **255**, 293 (2003).
[66] D. W. Hamby, D. A. Lucca, M. J. Klopfstein, and G. Cantwell, J. Appl. Phys. **93**, 3214 (2003).
[67] H. P. He, Z. Z. Ye, S. S. Lin, H. P. Tang, Y. Z. Zhang, L. P. Zhu, J. Y. Huang, and B. H. Zhao, J. Appl. Phys. **102**, 013511 (2007).
[68] T. C. Damen, S. P. S. Porto, and B. Tell, Phys. Rev. **142**, 570 (1966).
[69] K. Huang and A. Rhys, Proc. R. Soc. London A **204**, 406 (1950).
[70] J. J. Hopfield, J. Phys. Chem. Solids **10**, 110 (1959).
[71] O. Goede and E. Gutsche, Phys. Status Solidi B **17**, 911 (1966).
[72] D. J. Mowbray, O. P. Kowalski, M. S. Skolnick, M. Hopkinson, and J. P. R. David, Superlattice Microst. **15**, 313 (1994).
[73] K. J. Nash, M. S. Skolnick, P. A. Claxton, and J. S. Roberts, Phys. Rev. B **39**, R5558 (1989).
[74] R. Pecharroman-Gallego, Semicond. Sci. Technol. **22**, 1276 (2007).
[75] P. J. Dean, Phys. Status Solidi A **81**, 625 (1984).
[76] J. Gutowski, N. Presser, and I. Broser, Phys. Rev. B **38**, 9746 (1988).
[77] B. K. Meyer, J. Sann, S. Eisermann, S. Lautenschläger, M. R. Wagner, M. Kaiser, G. Callsen, J. S. Reparaz, and A. Hoffmann, Phys. Rev. B **82**, 115207 (2010).
[78] W. R. L. Lambrecht, A. V. Rodina, S. Limpijumnong, B. Segall, and B. K. Meyer, Phys. Rev. B **65**, 075207 (2002).
[79] J. Puls, F. Henneberger, and J. Voigt, Phys. Status Solidi B **119**, 291 (1983).
[80] T. Koida, S. F. Chichibu, A. Uedono, A. Tsukazaki, M. Kawasaki, T. Sota, Y. Segawa, and H. Koinuma, Appl. Phys. Lett. **82**, 532 (2003).
[81] Y. Zhong, A. B. Djurisic, Y. F. Hsu, K. S. Wong, G. Brauer, C. C. Ling, and W. K. Chan, J. Phys. Chem. C **112**, 16286 (2008).
[82] E. I. Rashba and G. E. Gurgenishvili, Sov. Phys. Solid State **4**, 759 (1962).
[83] F. Bertram, J. Christen, A. Dadgar, and A. Krost, Appl. Phys. Lett. **90**, 041917 (2007).
[84] O. Brandt, J. Ringling, K. H. Ploog, H.-J. Wünsche, and F. Henneberger, Phys. Rev. B **58**, R15977 (1998).
[85] W. Shan, X. C. Xie, J. J. Song, and B. Goldenberg, Appl. Phys. Lett. **67**, 2512 (1995).
[86] R. Heitz, C. Fricke, A. Hoffmann, and I. Broser, Mater. Sci. Forum **83**, 1241 (1992).
[87] D. L. Dexter, in *Solid State Physics*, edited by F. Seitz and D. Turnbull, Vol.6 (Academic, New York, 1958), p. 353.
[88] G. W. 't Hooft, W. A. J. A. van der Poel, L. W. Molenkamp, and C. T. Foxon, Phys. Rev. B **35**, R8281 (1987).
[89] E. I. Rashba, Sov. Phys. Semicond. **8**, 807 (1975).
[90] G. D. Sanders and Y.-C. Chang, Phys. Rev. B **28**, 5887 (1983).
[91] J. Bellessa, V. Voliotis, R. Grousson, X. L. Wang, M. Ogura, and H. Matsuhata, Phys. Rev. B **58**, 9933 (1998).
[92] V. A. Fonoberov and A. A. Balandin, J. Appl. Phys. **94**, 7178 (2003).
[93] V. A. Fonoberov and A. A. Balandin, Phys. Rev. B **70**, 195410 (2004).
[94] H. Karzel, W. Potzel, M. Köfferlein, W. Schiessl, M. Steiner, U. Hiller, G. M. Kalvius, D. W. Mitchell, T. P. Das, P. Blaha, K. Schwarz, and M. P. Pasternak, Phys. Rev. B **53**, 11425 (1996).
[95] S. Desgreniers, Phys. Rev. B **58**, 14102 (1998).
[96] F. Decremps, J. Pellicer-Porres, A. M. Saitta, J.-C. Chervin, and A. Polian, Phys. Rev. B **65**, 092101 (2002).
[97] J. S. Reparaz, L. R. Muniz, M. R. Wagner, A. R. Goni, M. I. Alonso, A. Hoffmann, and B. K. Meyer, Appl. Phys. Lett. **96**, 231906 (2010).
[98] G. Callsen, J. S. Reparaz, M. R. Wagner, R. Kirste, C. Nenstiel, A. Hoffmann, and M. R. Phillips, Appl. Phys. Lett. **98**, 061906 (2011).
[99] J. Wrzesinski and D. Fröhlich, Phys. Rev. B **56**, 13087 (1997).
[100] M. R. Wagner, G. Callsen, A. Hoffmann, and A. V. Rodina, (unpublished).
[101] J. S. Reparaz, F. Güell, M. R. Wagner, G. Callsen, R. Kirste, S. Claramunt, J. R. Morante, and A. Hoffmann, Appl. Phys. Lett. **97**, 133116 (2010).
[102] F. Leiter, H. Alves, D. Pfisterer, N. G. Romanov, D. M. Hofmann, and B. K. Meyer, Physica B **340**, 201 (2003).
[103] A. Janotti and C. G. V. de Walle, Phys. Rev. B **76**, 165202 (2007).
[104] P. J. Dean, A. D. Pitt, M. S. Skolnick, P. J. Wright, and B. Cockayne, J. Cryst. Growth **59**, 301 (1982).
[105] A. Naumov, K. Wolf, T. Reisinger, H. Stanzl, and W. Gebhardt, J. Appl. Phys. **73**, 2581 (1993).
[106] S. Fujii, T. Terada, Y. Fujita, and T. Iuchi, Jpn. J. Appl. Phys. **28**, 1712 (1989).
[107] A. Hoffmann, J. Christen, and J. Gutowski, Adv. Mater. Opt. Electron. **1**, 25 (1992).
[108] Y. T. Rebane and Y. G. Shreter, in *Springer Proceedings in Physics*, edited by J. H. Werner and H. P. Strunk, Vol. 54 (Springer, New York,1991), p. 28.
[109] J. W. Steeds, J. L. Batstone, Y. T. Rebane, and Y. G. Shreter, in *Springer Proceedings in Physics*, edited by J. H. Werner and H. P. Strunk, Vol. 54 (Springer, New York, 1991), p. 45.
[110] Y. T. Rebane, Phys. Rev. B **52**, 1590 (1995).
[111] Y. T. Rebane and J. W. Steeds, Phys. Rev. Lett. **75**, 3716 (1995).
[112] M. Kutrowski, T. Wojtowicz, G. Cywinski, L. V. Titova, E. Martin, X. Liu, J. K. Furdyna, and M. Dobrowolska, J. Appl. Phys. **97**, 013519 (2005).
[113] L. D. Landau and E. M. Lifshitz, *Quantum Mechanics*, Vol. 3 (Pergamon Press, New York, 1989), Chap. 11.
[114] C. Herring and M. Flicker, Phys. Rev. **134**, A362 (1964).